International Geology Review

ISSN: 0020-6814 (Print) 1938-2839 (Online) Journal homepage: http://www.tandfonline.com/loi/tigr20

Petrogenesis and mineralization of the Hulu Ni-Cu sulphide deposit in Xinjiang, NW China: constraints from Sr-Nd isotopic and PGE compositions

Dongmei Tang, Kezhang Qin, Benxun Su, Patrick Asamoah Sakyi, Yajing Mao & Shengchao Xue

To cite this article: Dongmei Tang, Kezhang Qin, Benxun Su, Patrick Asamoah Sakyi, Yajing Mao & Shengchao Xue (2014) Petrogenesis and mineralization of the Hulu Ni-Cu sulphide deposit in Xinjiang, NW China: constraints from Sr-Nd isotopic and PGE compositions, International Geology Review, 56:6, 711-733, DOI: 10.1080/00206814.2014.893413

To link to this article: https://doi.org/10.1080/00206814.2014.893413

International Geology Review, 2014
Vol. 56, No. 6, 711–733, http://dx.doi.org/10.1080/00206814.2014.893413

Taylor & Francis
Taylor & Francis Group

Petrogenesis and mineralization of the Hulu Ni-Cu sulphide deposit in Xinjiang, NW China: constraints from Sr-Nd isotopic and PGE compositions

Dongmei Tang[a]*, Kezhang Qin[a], Benxun Su[a], Patrick Asamoah Sakyi[b], Yajing Mao[a,c,d] and Shengchao Xue[a,d]

[a]*Key Laboratory of Mineral Resources, Institute of Geology and Geophysics, Chinese Academy of Sciences, Beijing 100029, China;* [b]*Department of Earth Science, University of Ghana, Legon-Accra, Ghana;* [c]*Xinjiang Research Centre for Mineral Resource, Xinjiang Institute of Ecology and Geography, Chinese Academy of Science, Urumqi 830011, China;* [d]*Institute of Geology and Geophysics, University of Chinese Academy of Sciences, Beijing 100049, China*

(*Received 27 September 2013; accepted 8 February 2014*)

The Permian Hulu intrusion is one of several sulphide-bearing Permian mafic–ultramafic intrusions in the eastern part of the eastern Tianshan located at the southern margin of the Central Asian Orogenic Belt (CAOB) in Xinjiang, NW China. The intrusion is composed of lherzolite, olivine websterite, gabbro, and gabbro-diorite. Disseminated and net-textured Ni-Cu sulphide ores are located at the bottom of the lopolith complex. Negative Zr, Hf, Nb, and Ta anomalies, whole-rock $\varepsilon Nd(t)$ values of +5.7 to +8.8, and variable $(Th/Nb)_{PM}$ values (from 1.06 to 8.13) suggest that the source of the Hulu complexes is depleted mantle metasomatized by subducted slab-derived fluid and/or melt (~5% global subducted sediment and 15% slab fluid) that has experienced approximately 3% lower crustal and 10% upper crustal contamination. The Hulu intrusion is characterized by low PGE abundances i.e. 0.03–1.08 ppb Ir, 0.04–0.69 ppb Ru, 0.02–2.15 ppb Rh, 0.30–48.71 ppb Pt, and 0.21–344 ppb Pd. Our calculations indicate that if the Pd, Os, Ir, and Cu contents of the primary magma were 2.1 ppb, 0.03 ppb, 0.05 ppb, and 200 ppm, respectively, a variable R-factor between 200 and 1600 with residual magma that had experienced 0.01% early-sulphide segregation can explain the variation in Pd, Os, and Ir contents of sulphide-poor and disseminated sulphide samples of the Hulu deposit. Basaltic magma fractionation and assimilation and/or contamination of sulphur-bearing crustal materials might have triggered sulphur saturation to form Cu-Ni sulphide ores. Tarim basaltic PGE contents cannot be used as the mineralized parent magma for the Hulu intrusion because of the differing evolutionary trends of the Ni/Pd and Cu/Ir values. However, similar Cu/Ni and Pd/Ir values in Tarim basalts and Hulu Cu-Ni sulphide ores, as well as the same early sulphide segregation process, show that certain genetic relationships between them and magma sources are probably similar to each other.

Keywords: Hulu magmatic sulphide deposit; platinum-group elements; early sulphide segregation; crustal contamination; Eastern Tianshan

Introduction

An economically significant Cu-Ni metallogenic belt is located in Eastern Tianshan area, in the southern part of the Central Asian Orogenic Belt (CAOB) (Mao *et al.* 2002; Qin *et al.* 2003; Su *et al.* 2013). In the Eastern Tianshan and its adjacent area, there are several series of mafic–ultramafic intrusions (e.g. Tulaergen, Xiangshan, Huangshan, Tianyu, Baishiquan, Poyi, and Hongshishan), most of which host copper-nickel mineralization. They can be divided into three mafic–ultramafic intrusion belts: Eastern Tianshan, Central Tianshan, and Beishan. In the Eastern Tianshan belt, there are the Tulaergen, Huangshan, Xiangshan, Hulu, Mati, and Chuanzhu mafic–ultramafic related magmatic sulphide deposits. The mid-sized Baishiquan and Tianyu deposits are located in the Central Tianshan belt, whereas the Poshi, Poyi, Podong, Luodong, and Hongshishan deposits are found in the Beishan belt. These magmatic sulphide deposits are early Permian, ranging from 285 Ma to 279 Ma (Mao *et al.* 2002; Han *et al.* 2004; Zhou *et al.* 2004; Wu *et al.* 2005; Zhang *et al.* 2008; Tang *et al.* 2011).

The tectonic background of these magmatic Cu-Ni sulphide deposits in the Palaeozoic CAOB is different from that of most world-class magmatic Cu-Ni-PGE sulphide deposits. The CAOB was formed by multiple subduction–accretion and collision processes from the Neoproterozoic to the late Palaeozoic (Sengör *et al.* 1993; Jahn *et al.* 2004; Xiao *et al.* 2004, 2009; Windley *et al.* 2007). At present, global large magmatic sulphide deposits are mostly located in the Archaean or Proterozoic craton (Bushveld layer intrusion in Kaapvall craton, Voisey's deposit in the Archaean Nain Province and Proterozoic Churchill Province, Maier and Barnes 1998; Brenan and Li 2000; Li *et al.* 2001; Ripley *et al.* 2002), and/or Large Igneous Province (LIP) (Duluth deposit in Keweenawan flood basalt province, Noril'sk deposit in Siberia LIP, Emeishan in Emeishan LIP, Ripley *et al.* 2003; Lightfoot and Keays 2005; Song *et al.* 2006). What is the role of subduction and collision in the

*Corresponding author. Email: tdm@mail.iggcas.ac.cn

magma emplacement and mineralization processes? Are magmatic Cu-Ni sulphide deposits in the CAOB special types occurring in the orogen or not? And what is their relationship with Tarim LIP near the Eastern Tianshan area?

The Sr-Nd isotopic features of mafic–ultramafic magmas offer important constraints on their source characteristics and tectonic setting. PGEs are mainly concentrated in primary magmatic sulphides (Naldrett 1989, 2004; Barnes and Maier 1999; Maier 2005). Therefore, PGEs are potentially useful trace elements for studying the early history of the earth and the origin of magmatic Ni-Cu sulphide deposits, and the petrogenesis of mafic–ultramafic rocks and associated sulphide-ore formation.

This paper, therefore, attempts to identify the whole-rock Sr-Nd isotopic characteristics and PGE geochemical characteristics, as well as sulphide and whole-rock S isotopic characteristics of the Hulu mafic–ultramafic intrusion in Eastern Tianshan and then compare the PGE characteristics to the Emeishan basalt and Ni-Cu sulphide deposits related to the Emeishan LIP. Furthermore, this study discusses the formation background and key factors such as parent magma characteristics, crustal contamination, and sulphide segregation that control the emplacement and mineralization of the Hulu magmatic Ni-Cu sulphide deposits in Eastern Tianshan.

Geological background

The CAOB, extending over 5000 km from west to east, represents the world's largest late Palaeozoic accretionary orogenic belt located between the Siberian Craton in the north and the Tarim Craton and North China Craton in the south (Figure 1, Sengör *et al.* 1993; Xiao *et al.* 2004, 2009; Windley *et al.* 2007; Wong *et al.* 2010; Rojas-Agramonte *et al.* 2011).

The Eastern Tianshan Cu-Ni metallogenic belt, set between the Junggar and Tarim blocks, forms the eastern part of the Tianshan Mountains, and mainly consists of three tectonic units: the Bogeda-Haerlike Belt in the north, Jueluotage Belt in the centre, and Middle Tianshan Terrane in the south. It was formed by multiple subduction–accretion and collision processes from the Neoproterozoic to the late Palaeozoic (Sengör *et al.* 1993; Jahn *et al.* 2004; Xiao *et al.* 2004, 2009; Windley *et al.* 2007), and is a composite orogenic belt comprising fragments of Precambrian microcontinents, Palaeozoic island arcs, ophiolite, and successions of volcanic rocks (Figure 1(a); Coleman 1989; Sengör *et al.* 1993; Jahn *et al.* 2000; Windley *et al.* 2002).

The Jueluotage Belt can be subdivided, from north to south, into the Wutongwozi–Xiaorequanzi intra-arc basin, Dananhu–Tousuquan island arc, Kangguer–Huangshan ductile shear zone, and Yamansu back-arc basin (Qin *et al.* 2002), all of which are separated by several major faults (Wutongwozi–Tousuquan fault, Kanggurtage–Huangshan fault, Kushui fault, and Shaquanzi fault; Figure 1(b); Qin *et al.* 2002; Xu *et al.* 2006; Su *et al.* 2011, 2012). Many subsidiary faults are also well developed within each tectonic unit.

The Hulu Cu-Ni sulphide-bearing mafic–ultramafic intrusion occurs in the eastern part of the Eastern Tianshan (Figure 1(a)). It occurs in the NEE- or ENE-trending Kangguer–Huangshan fault (Figure 1(b)), close to the northern edge of the Tarim block. The ENE-trending faults and tight folds are the most developed structures in the Kangguer–Huangshan ductile shear belt.

The strata of the Kangguer–Huangshan area are felsic-mafic volcanic rocks and pyroclastic rocks of the Late Devonian Dananhu group; felsic volcanic rocks, pyroclastic rocks interbedded with fine-grained clastic rocks, and limestone of the late Carboniferous Yamansu group; granulite, schist, slate, and limestone of the Gandun group; and felsic and mafic volcanic rocks, siliceous rocks, slate, limestone, and schist of the late Carboniferous Wutongwozi group. There is also a thin cover of Cenozoic argillaceous sandstone, calcareous siltstone, and fine-grained sandstone; Quaternary conglomerates; and an alluvial layer in this area (Figure 1(b)).

Three stages of magmatism produced early Carboniferous granodioritic intrusions, slightly younger granitic intrusion, and early Permian mafic–ultramafic intrusions emplaced in the Wutongwozi and Gandun groups.

Geology of the Hulu magmatic Ni-Cu sulphide deposits

The Hulu intrusion occurs as two irregular circular bodies, extending to about 1400 m in length and 340–720 m in width with an outcrop area of 0.75 km^2 (Figure 2(a)). The cross-sectional shape resembles an asymmetric lopolith (Figure 2(b) and (c)). The Hulu intrusion is mainly composed of diorite, gabbro-diorite, gabbro, olivine websterite, plagioclase-bearing olivine websterite, and lherzolite. Lherzolite is dominant. All the rocks of the fracture-controlled intrusive body exhibit gradational contact with each other and with the country rocks in the eastern part of the intrusion. Quartz hornblende plagioclase granulite, sericite quartzite, amphibolite schist, and metarhyolite of the Lower Carboniferous Wutongwozi group are the immediate wall rocks of the Hulu intrusion (Figure 2(a)).

Lherzolite crops out in the centre and accounts for 80% of the volume of the intrusion. The lherzolite contains 50–75% olivine and 20–25% pyroxene (clinopyroxene and orthopyroxene), plus minor hornblende (~3%), phlogopite (~1%), and spinel inclusions within some olivine crystals (Figure 3(a)). The olivine websterite occurs in banded forms and is distributed around the edge and at the bottom of the lherzolite. The volume of the olivine websterite is about 5–8% of the intrusion. The major

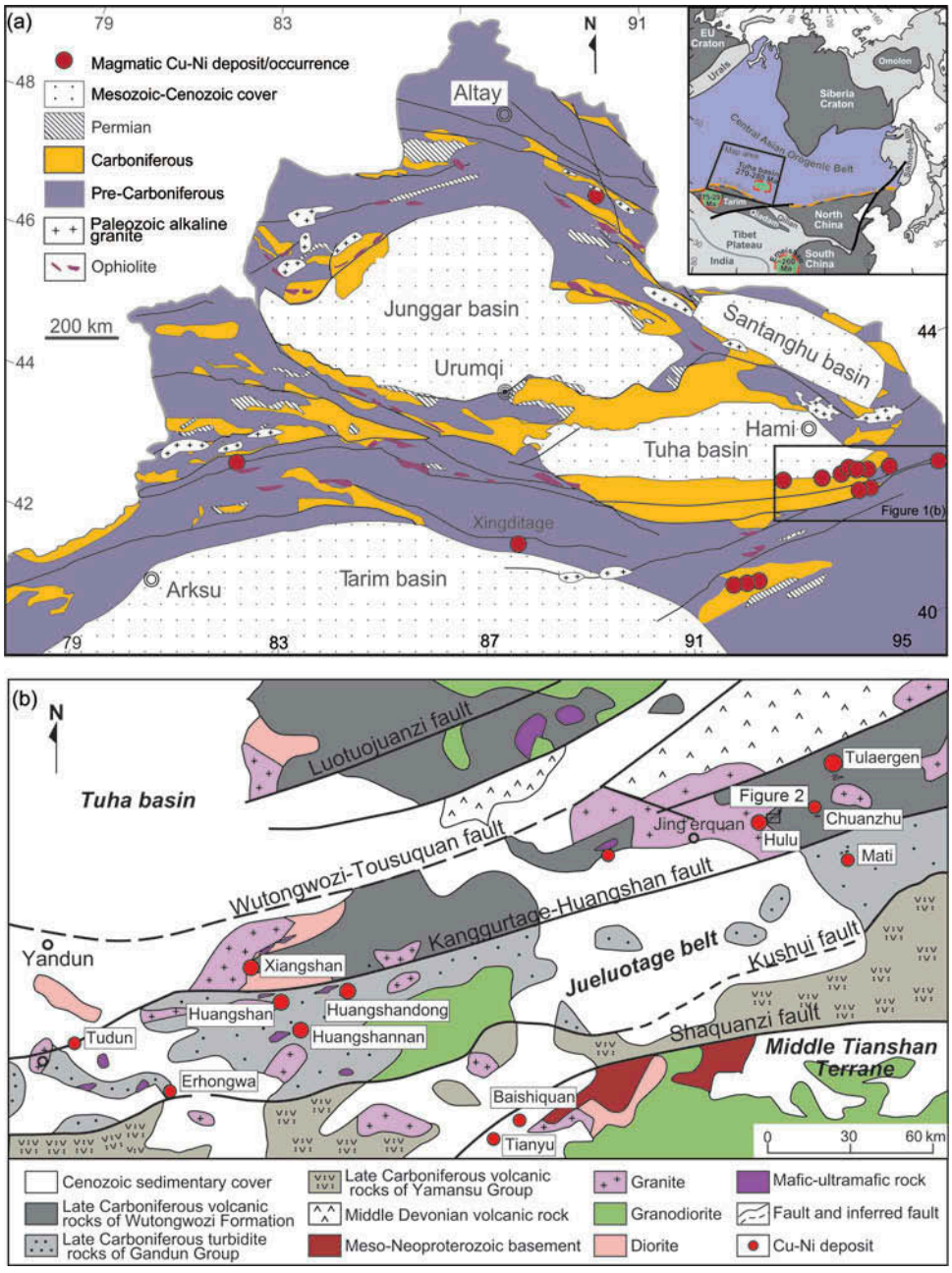

Figure 1. (a) Tectonic units and location of magmatic Ni-Cu sulphide deposits in northern Xinjiang, modified from Jahn *et al.* (2004), Xiao *et al.* (2009), and Li *et al.* (2012c). (b) Distribution of Ni-Cu deposits/occurrences associated with mafic–ultramafic intrusions in the eastern part of the Eastern Tianshan, modified from Qin *et al.* (2003).

silicate minerals are olivine (35–50%), clinopyroxene and orthopyroxene (30–40%), plagioclase (5–15%), hornblende (5–10%), and minor spinel, sphene, apatite, and magnetite. The olivine is anhedral to subhedral and is commonly enclosed by large clinopyroxene or orthopyroxene crystals (Figure 3(b)). The boundary between olivine websterite and lherzolite is a transition zone.

The gabbro is characterized by the interlocking of randomly oriented tabular plagioclase (40–55%) and anhedral pyroxene (45–55%) (Figure 3(c) and (d)). Minor olivine, hornblende, phlogopite, and Fe-Ti oxides are also present in the gabbroic rocks. The gabbro-diorite is also characterized by a granular texture (Figure 3(e) and (f)). In addition to plagioclase (35–45%), pyroxene (15–20%) and hornblende (30–40%), biotite, and a small amount of quartz are also present.

The sulphide mineralization occurs predominantly as disseminated and net-textured sulphides in the

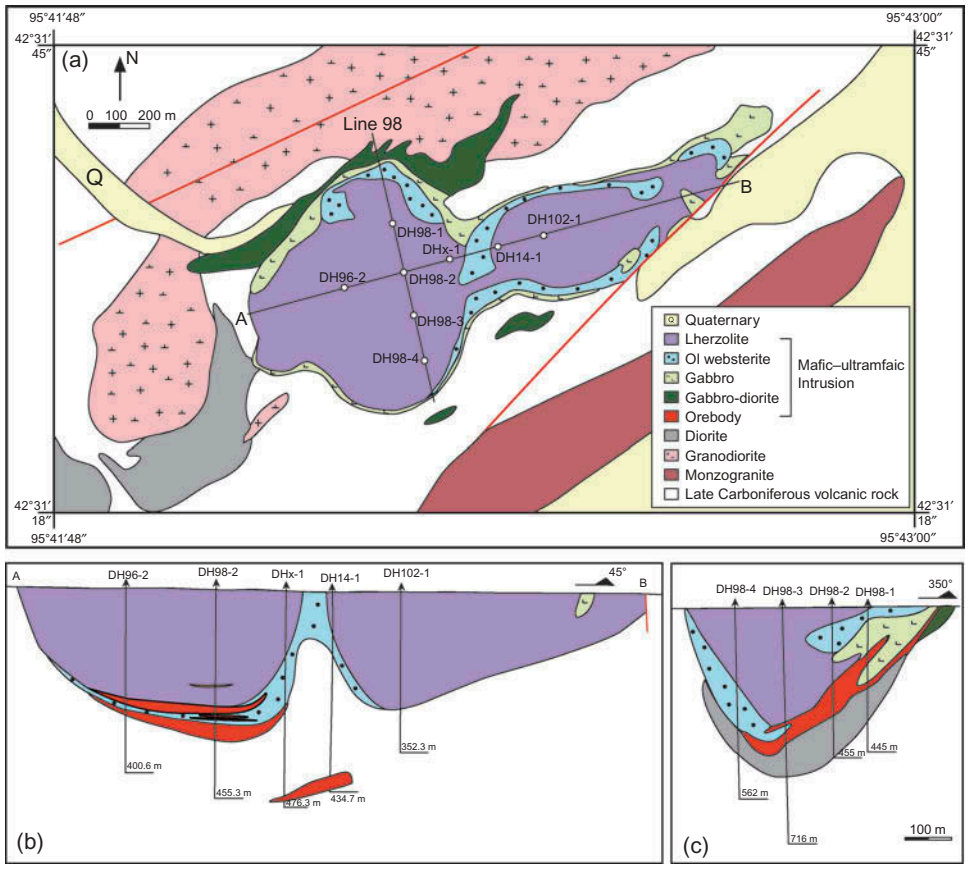

Figure 2. (a) Simplified geologic map of the Hulu region. Cross-sections (b) and (c) of the Hulu intrusion.

interstices of ultramafic minerals (Figure 4(a) and (b)). Other ore structures are massive, semi-massive (Figure 4 (c) and (d)), sparsely disseminated, and banded. The main ore-bearing rocks in the Hulu deposit are olivine websterite and lherzolite. The gabbro-diorite and diorite are almost barren, whereas the sulphide-bearing olivine websterites are mostly altered. Apart from a few olivine websterite and lherzolite samples that have experienced different degrees of serpentinization and tremolitization, most other samples are fresh or weakly altered. Pyrrhotite, pentlandite, and chalcopyrite are the most important phases in the sulphide ores (Figure 4(a)–(d)). Currently, Ni metal resources are estimated at 0.08 Mt, Cu metal resources is 0.05 Mt, and the average tenors of Ni and Cu are 0.44 wt.% and 0.37 wt.%, respectively.

Alteration is common in the Hulu intrusion. Olivine is mostly altered to serpentine, which is associated with magnetite, whereas orthopyroxene is partially altered to talc and chlorite. Similarly, clinopyroxene is partially altered to actinolite or tremolite, and plagioclase is partly altered to sericite, epidote, and albite. Secondary magnetite and pyrite are present in some sulphide mineralized samples.

Samples and analytical methods

The samples for this study were collected from mineshaft adits at elevations of 925 m, 965 m, 1005 m, and 1090 m (Figure 5). The corresponding depths from the surface are 538 m, 498 m, 358 m, and 273 m, respectively. The samples selected for this study are fresh unmineralized or mineralized with disseminated up to massive sulphides.

Whole-rock major and trace element analyses

The collected samples were powdered in an agate mortar. Major elements were analysed on fused glass discs with an X-ray fluorescence spectrometer (Shimadzu XRF-1500) at the Institute of Geology and Geophysics, Chinese Academy of Sciences (IGGCAS), Beijing, China. The loss-on-ignition (LOI) was measured as the weight loss of the samples after 1 h baking at a constant temperature of 1000°C. The powdered samples, weighing approximately 1.2 g, were fused with lithium tetraborate ($Li_2B_4O_7$, 6 g) at 1050°C for 20 min. The precision for major elements was better than 2% relative to standard. The accuracy and reproducibility were monitored by the Chinese national standard sample GSR3, with relative standard deviation better than 1%.

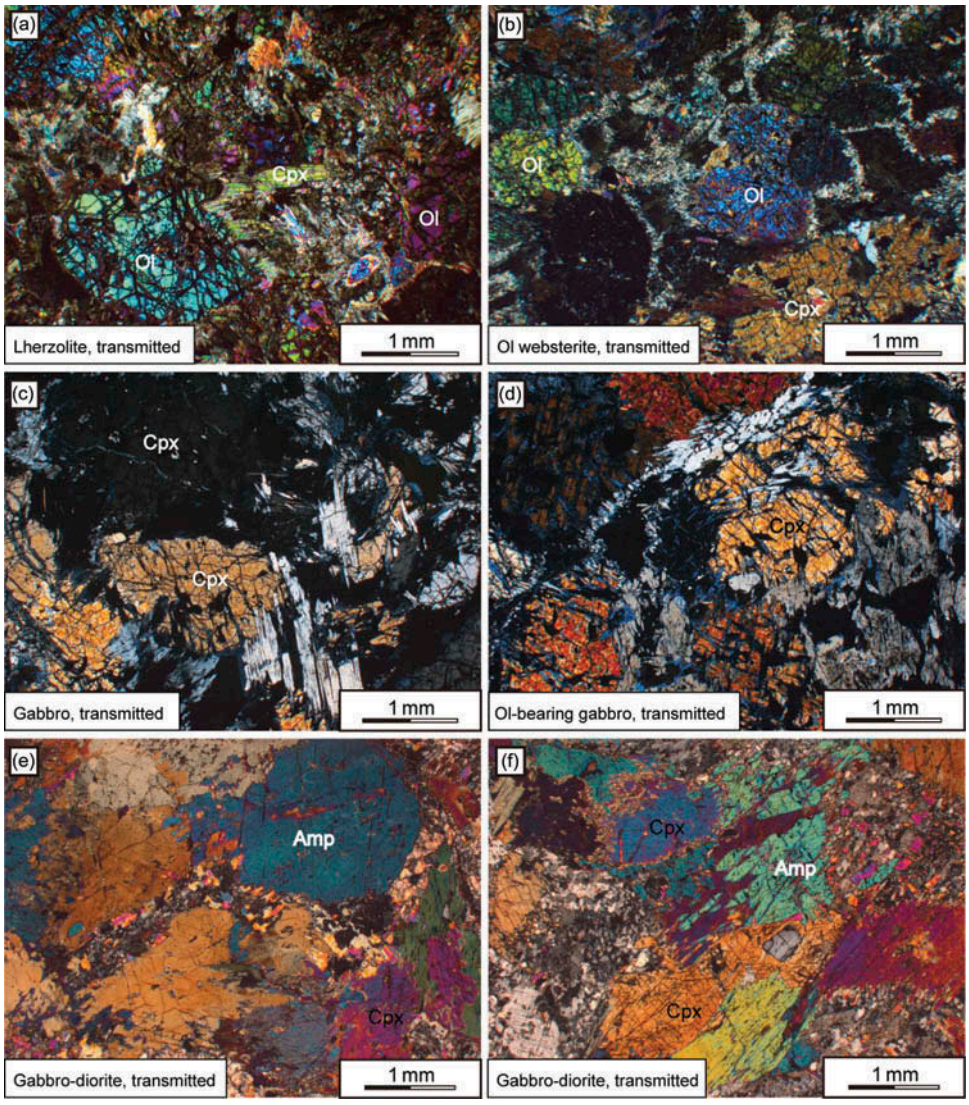

Figure 3. Photomicrographs showing the textures of the major rock types in the Hulu intrusion. Opx, orthopyroxene; Ol, olivine; Cpx, clinopyroxene; Hb, hornblende; Pl, plagioclase.

Trace elements were determined using an ELEMENT inductively coupled plasma mass spectrometer (ICP-MS) at IGGCAS. The powders (40 mg) were dissolved in 1 ml distilled HF and 0.5 ml distilled HNO_3 in Teflon screw-cap capsules. The solutions were heated at 170°C for 10 days, then dried and re-dissolved with 2 ml HNO_3 in the capsules. Finally, the solutions were diluted to 50 ml in 1% HNO_3 before analysis. The precision for trace elements was better than 5% relative to standard. The standard sample GSR3 was used to monitor the analytical accuracy and reproducibility, with relative standard deviation better than 3%. Major and trace element data are listed in Table 1.

Ni, Cu, and PGE contents

The PGE concentrations of the sulphide mineralized samples were determined by the combination of NiS bead preconcentration, Te co-precipitation, and ICP-MS analysis in the National Research Centre for Geo-Analysis, Beijing, following detailed procedures reported in Sun *et al.* (1997). The PGE contents in sulphide-poor samples were determined by the Carius tube digestion and isotope dilution ICP-MS technique at the Institute of Geochemistry, Chinese Academy of Sciences, in Guiyang. The detailed procedures of this technique, blank concentrations, and detection limits are described in Qi *et al.* (2007).

Sr-Nd isotopes

Rb-Sr and Sm-Nd isotopes were determined at IGGCAS using an IsoProbe-T thermal ionization mass spectrometer, following the procedures described in Chu *et al.* (2009). Procedural blanks were 40 pg for Rb, 300 pg for Sr, 20 pg

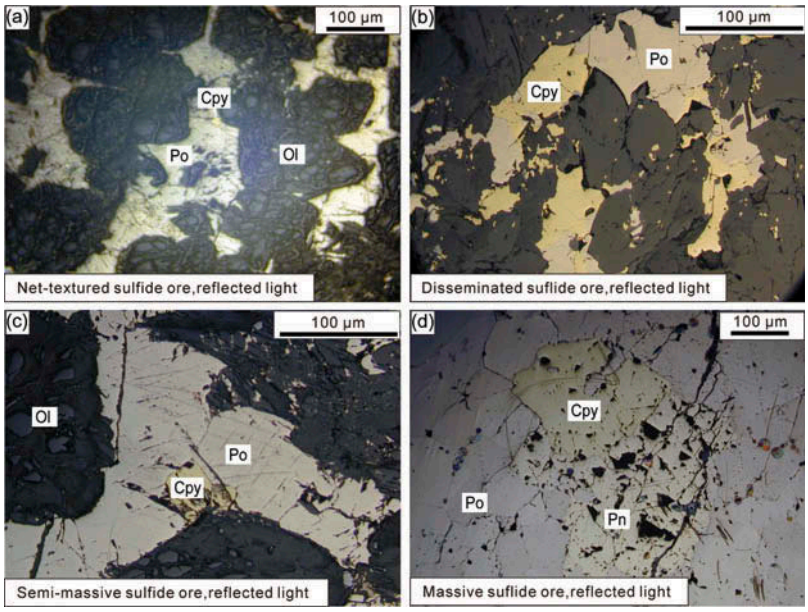

Figure 4. Microphotographs showing the textures of net-textured sulphide (a), disseminated sulphide (b), semi-massive sulphide (c), and massive sulphide (d) ores in the Hulu intrusion. Cpy, chalcopyrite; Pn, pentlandite; Po, pyrrhotite. Other mineral abbreviations are as in Figure 3.

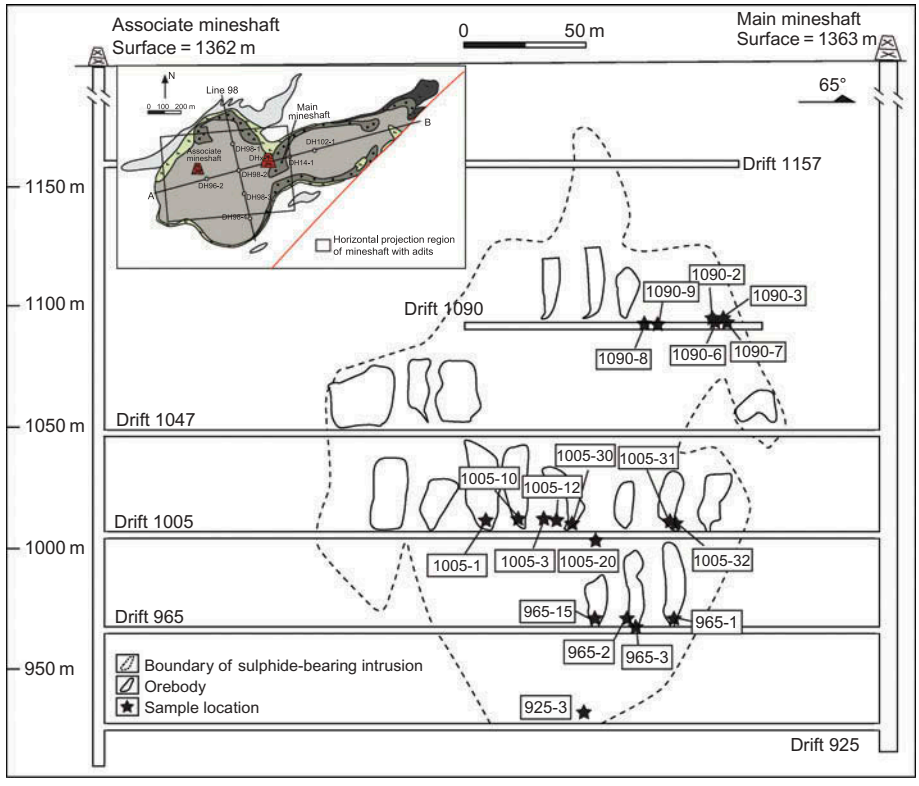

Figure 5. Vertical projection of mineshaft with adits and sample locations.

for Sm, and 60 pg for Nd. Sr and Nd isotopic ratios were corrected for mass fractionation relative to $^{86}Sr/^{88}Sr = 0.1194$ and $^{146}Nd/^{144}Nd = 0.7219$, respectively. Typical within-run precision (2σ) for Sr and Nd isotopic ratios was better than ±0.5%. The measured values for the NBS-987 Sr standard and the JNdi-1 Nd standard were

Table 1. Whole-rock major and trace element compositions of the Hulu mafic–ultramafic intrusion.

Sample No.	925-3	1090-2	1090-3	1090-6	1090-7	1090-9	1090-8	1005-32	1005-31	965-2	1005-20	965-3
Rock	Diorite	Gabbro-diorite				Gabbro		Ol websterite				
Mineralization		Sulphide-poor				Sulphide-poor		Disseminated sulphide			Sulphide-poor	Massive
Major oxides (wt.%)												
SiO2	55.74	51.60	51.12	51.67	53.23	48.10	47.30	40.20	41.20	41.54	40.70	40.79
TiO2	0.60	1.35	1.09	1.06	1.00	0.85	0.95	0.47	0.41	1.53	0.60	0.41
Al2O3	14.13	15.97	16.49	15.94	17.65	14.00	13.50	6.050	3.23	6.63	5.95	5.34
TFe2O3	8.76	8.98	8.20	7.08	6.21	7.80	7.41	14.30	19.90	16.87	12.80	18.20
MnO	0.15	0.16	0.15	0.11	0.09	0.17	0.17	0.17	0.15	0.2	0.16	0.15
MgO	5.53	6.91	6.66	7.92	5.18	10.2	13.3	27.6	26.8	22.0	27.3	24.2
CaO	7.78	10.05	11.7	9.68	10.27	10.2	10.7	3.35	1.33	7.12	3.45	3.06
Na2O	3.83	2.93	2.85	4.38	4.47	2.85	2.37	0.69	0.57	0.28	0.60	0.19
K2O	1.35	1.06	0.79	0.56	0.36	0.79	0.80	0.43	0.40	0.06	0.45	0.04
P2O5	0.15	0.28	0.22	0.26	0.096	0.05	0.04	0.06	0.03	0.16	0.08	0.08
LOI	0.07	0.11	0.06	0.01	0.01	4.15	3.23	1.56	2.37	0.01	6.75	0.07
S	0.67	0.48	0.44	0.94	1.12	0.08	0.21	5.77	3.92	3.29	0.05	6.87
Total	98.8	99.9	99.8	99.6	99.7	99.3	100.0	100.7	100.3	99.6	98.9	99.4
Trace elements (ppm)												
Li	27.0	26.1	20.5	23.7	14.2	26.9	7.37	12.7	6.61	1.85	47.0	3.95
Be	1.31	1.21	1.2	1.14	1.47	1.79	0.732	0.895	0.474	0.424	1.08	0.37
Sc	20.8	23.7	26.4	19.4	27.9	40.5	37	15.8	39.7	31.9	23.7	13.04
V	166	163	170	131	145	348	262	146	297	196	153	76.5
Cr	283	234	333	462	200	215	460	1331	31.1	431	444	197.68
Co	25.7	35.5	30.2	33.3	27.3	43	142	104	42.2	95.7	55.5	270
Ni	60.1	80.7	88.2	255	113	142	475	952	39.5	282	320	5184
Cu	28.4	29	28.8	52.1	87.5	47	1677	233	174	15.8	102	2325
Zn	57.4	74.4	74.1	46.5	54.2	131	172	118	72.8	82.1	103	81.9
Ga	17.5	16	16.9	13.8	18.5	23.9	10.7	11.1	17.6	10.5	12.9	7.74
Rb	54.6	41.6	31.2	16.3	13.6	28.5	10.6	8.21	6.15	0.736	26.2	0.60
Sr	414	388	466	1258	989	112	152	235	563	25.7	424	72.6
Y	14.3	24.7	22.7	18.4	19.5	16.5	16.6	20.8	12.9	13.1	17.0	11.9
Zr	38.4	64.2	59.4	90.7	93.9	29	14.7	69.3	25.0	35.6	69.9	47.76
Nb	3.57	4.98	4.03	4.60	3.03	4.80	3.12	2.79	1.61	1.65	3.05	2.04

(*Continued*)

Table 1. (Continued).

Sample No.	925-3	1090-2	1090-3	1090-6	1090-7	1090-9	1090-8	1005-32	1005-31	965-2	1005-20	965-3
Rock	Diorite	Gabbro-diorite				Gabbro		Ol websterite				
Mineralization		Sulphide-poor				Sulphide-poor		Disseminated sulphide			Sulphide-poor	Massive
Cs	5.24	4.38	3.80	3.66	1.59	3.33	1.50	2.02	0.147	0.055	3.51	0.62
Ba	223	180	133	122	107	107	97.4	138	106	3.60	120	43.37
La	9.08	12.2	11.3	10.7	7.63	14.0	10.8	6.20	5.24	12.9	10.2	4.26
Ce	19.4	27.7	27.7	27.4	18.7	26.6	23.8	15.6	12.2	26.2	23.9	10.05
Pr	2.74	3.93	3.85	4.01	2.83	3.22	3.20	2.18	1.79	3.39	3.42	1.45
Nd	12.0	17.0	15.9	18.2	13.5	12.7	13.6	8.80	8.37	14.7	16.0	6.40
Sm	2.43	4.18	3.72	4.21	3.21	2.58	2.95	2.2	2.4	3.33	3.42	1.73
Eu	0.798	1.26	1.40	1.41	1.32	0.949	0.675	0.98	0.853	0.804	1.19	0.94
Gd	2.61	3.91	3.89	3.78	3.45	2.61	2.99	3.39	2.26	3.26	3.30	1.84
Tb	0.422	0.713	0.656	0.619	0.615	0.501	0.505	0.396	0.371	0.554	0.583	0.320
Dy	2.50	4.45	4.02	3.59	3.72	3.00	3.02	2.57	2.33	2.99	3.32	2.03
Ho	0.462	0.827	0.789	0.651	0.729	0.611	0.605	0.583	0.483	0.523	0.629	0.45
Er	1.45	2.44	2.13	1.93	2.01	1.92	1.81	2.08	1.35	1.34	1.88	1.29
Tm	0.235	0.356	0.347	0.282	0.306	0.313	0.304	0.214	0.197	0.185	0.284	0.21
Yb	1.36	2.04	2.09	1.57	1.82	1.91	1.89	1.39	1.26	1.07	1.69	1.36
Lu	0.197	0.311	0.301	0.236	0.263	0.294	0.295	0.193	0.194	0.136	0.263	0.21
Hf	1.33	1.73	1.58	2.39	2.61	1.04	0.684	2.26	0.982	1.28	1.94	1.43
Ta	0.24	0.328	0.24	0.272	0.189	0.380	0.188	0.301	0.100	0.319	0.194	0.170
Pb	9.42	8.45	9.49	13.4	9.94	4.25	1.80	2.02	1.87	1.80	7.70	6.72
Th	0.943	1.47	1.23	1.13	0.416	2.83	1.75	0.853	0.355	1.60	1.08	1.15
U	1.51	0.570	0.453	0.351	0.971	0.925	0.547	0.552	0.164	0.442	0.785	0.315

Sample No.	1005-1	1005-12	1005-10	965-1	1005-3	965-15	1055-30
Rock	Pl-bearing lherzolite		Lherzolite				
Mineralization	Disseminated sulphide	Sulphide-poor	Sulphide-poor	Net-textured sulphide	Disseminated sulphide		
Major oxides (wt.%)							
SiO_2	36.70	38.30	37.80	37.70	38.56	36.23	33.10
TiO_2	1.48	0.12	0.17	0.42	1.49	1.27	0.30
Al_2O_3	5.12	3.18	3.84	5.43	4.79	4.92	3.16
TFe_2O_3	21.0	13.3	13.3	16.5	16.3	18.6	28.3
MnO	0.32	0.17	0.16	0.15	0.25	0.29	0.16
MgO	26.6	36.6	35.6	28.0	27.7	28.0	24.6
CaO	4.44	1.85	1.61	1.97	3.97	3.87	1.78
Na_2O	0.58	0.34	0.57	0.71	0.37	0.42	0.43
K_2O	0.084	0.11	0.12	0.34	0.10	0.085	0.22
P_2O_5	0.11	0.03	0.03	0.10	0.13	0.12	0.06
LOI	2.70	5.88	6.85	5.53	5.50	3.10	3.27
S	1.33	0.19	0.09	3.30	1.27	3.10	4.23
Total	100.4	100.1	100.1	100.2	100.4	99.9	99.6

(*Continued*)

Table 1. (Continued).

Sample No.	1005-1	1005-12	1005-10	965-1	1005-3	965-15	1055-30
Rock	Pl-bearing lherzolite		Lherzolite				
Mineralization	Disseminated sulphide	Sulphide-poor	Sulphide-poor	Net-textured sulphide	Disseminated sulphide		
Trace elements (ppm)							
Li	7.86	61.1	41.1	4.63	5.06	4.34	4.25
Be	1.18	0.922	0.969	0.320	0.830	0.864	0.260
Sc	20.0	21.5	25.1	30.6	18.9	16.1	41.3
V	150	126	161	342	146	137	339
Cr	44.0	406	456	185	144	268	245
Co	124	62.8	55.6	43.6	110	130	49.8
Ni	90.0	364	302	22.0	381	166	42.1
Cu	68.1	91.8	180	69.8	73.1	61.5	43.8
Zn	118	99.0	85.3	121	93.5	101	99.4
Ga	7.79	12.8	13.3	29.7	9.17	7.84	26.3
Rb	2.03	115	28.5	15.4	4.09	3.02	9.78
Sr	223	364	436	752	213	143	669
Y	15.3	16.2	16.7	15.6	18.2	14.6	10.3
Zr	86.8	56.6	85.3	43.9	114	82.7	34.7
Nb	2.27	2.67	3.32	1.71	3.84	2.75	1.84
Cs	0.25	17.7	4.71	1.13	0.454	0.262	1.20
Ba	29.7	145	86.7	184	29.9	52.6	148
La	5.12	10.2	14.3	5.84	8.65	6.46	5.73
Ce	14.3	22.6	29.9	17.2	22.3	16.7	18.2
Pr	2.21	2.93	3.65	2.33	3.37	2.48	2.18
Nd	10.7	13.0	15.1	10.1	15.5	11.9	9.49
Sm	2.82	3	3.46	3.39	3.78	2.91	2.76
Eu	0.859	1.09	1.25	1.25	1.02	0.893	0.78
Gd	2.86	3.01	3.11	3.69	3.55	2.86	2.17
Tb	0.479	0.558	0.568	0.545	0.639	0.505	0.33
Dy	2.90	3.06	3.33	3.40	3.59	2.71	2.16
Ho	0.560	0.614	0.642	0.615	0.668	0.529	0.405
Er	1.55	1.82	1.89	1.99	1.86	1.55	1.33
Tm	0.213	0.264	0.292	0.255	0.279	0.213	0.165
Yb	1.36	1.65	1.74	1.78	1.65	1.21	1.18
Lu	0.193	0.239	0.268	0.260	0.257	0.198	0.170
Hf	2.02	1.82	2.44	1.42	2.51	2.00	1.05
Ta	0.131	0.185	0.227	0.15	0.246	0.168	0.195
Pb	3.02	8.32	7.95	3.12	3.00	2.25	2.26
Th	0.287	1.11	1.10	1.33	0.906	0.468	1.23
U	0.101	1.12	1.02	0.240	0.298	0.223	0.270

$^{87}Sr/^{86}Sr$ = 0.710246 ± 11 (2σ, n = 8) and $^{143}Nd/^{144}Nd$ = 0.512113 ± 12 (2σ, n = 8), respectively. During data collection, a USGS reference material BCR-2 was measured for Rb-Sr and Sm-Nd isotopic composition to monitor the accuracy of the analytical procedures, and the results obtained were: 46.53 ppm Rb, 367.31 ppm Sr, $^{87}Sr/^{86}Sr$ = 0.704965 ± 3 (2σ), 6.483 ppm Sm, 27.60 ppm Nd, and $^{143}Nd/^{144}Nd$ = 0.512671 ± 10 (2σ) (0.512641 ± 18, Raczek *et al.* 2001).

Sulphur isotope

We selected disseminated sulphide ores, pyrrhotite, pentlandite, and chalcopyrite in sulphide-bearing samples, as well as tuff (country rock) powder and pyrite of Hulu deposits, using MAT253 gas isotopic mass spectrometry to analyse the sulphur isotope component. CDT was measured by the standard denoted δ^{34}SV-CDT. Analysis accuracy is better than ±0.2‰. Sulphide reference standards were the GBW-04414 and GBW-04415 silver sulphide standards, and their $\delta^{34}S$ values were –0.07 ± 0.13‰ and 22.18 ± 0.14‰, respectively.

Results

Silicate minera and, whole-rock major and trace elements

There are two kinds of olivine forsterite (Fo) in the Hulu intrusion, major olivine characterized by Fo 79–86, and minor olivine with a composition of Fo 68–78. The higher Fo olivine occurs in all lherzolite and most olivine websterite. The olivine with lower Fo contents occurs in the websterite, gabbro, and gabbro-diorite. The contents of Ni in olivine range from 150 ppm to 1300 ppm. There are no correlations between Fo and Ni contents of olivine. Orthopyroxene from the ultramafic unit of the Hulu intrusion has a composition similar to bronzite. The $Mg^{\#}$ (100 Mg/(Mg + Fe), molar) of clinopyroxene from the Hulu intrusion ranges from 79 to 92, and exhibits similar composition to augite and enstatite. The plagioclase from the Hulu intrusion is characterized by An contents ranging from 55 to 75.

The MgO contents of olivine websterite and lherzolite are 22.0–27.6 wt.% and 24.6–36.6 wt.%, respectively. The lherzolite samples have higher MgO and lower SiO_2 contents than those of olivine websterite (Figure 6(a)). The gabbros contain 10.2–13.3 wt.% MgO, 7.41–7.80 wt.%

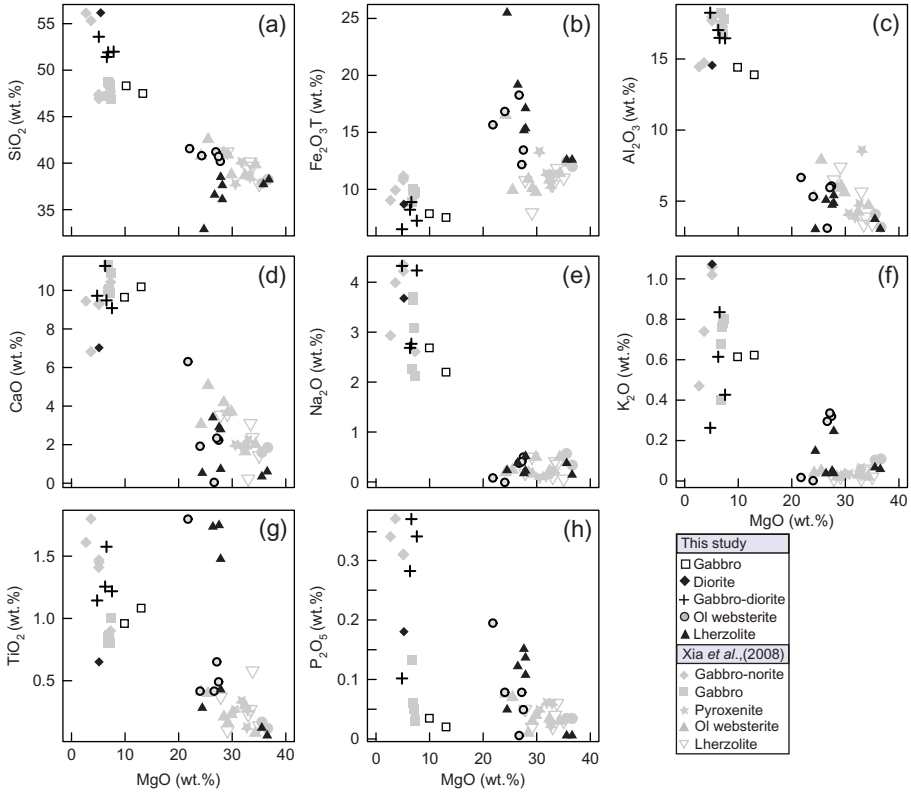

Figure 6. Harker plots of whole-rock compositions of the Hulu mafic–ultramafic intrusion.

Fe_2O_3T, 13.5–14.0 wt.% Al_2O_3, and 10.2–10.7 wt.% CaO (Figure 6(b)–(d)). The Na_2O and K_2O contents of gabbro and gabbro-diorite are higher than those of lherzolite and olivine websterite (Figure 6(e) and (f)). The contents of TiO_2 in the ultramafic and gabbroic rocks range from 0.12 wt.% to 1.53 wt.% (Figure 6(g)).

With the exception of two mineralized samples that show high total iron oxide contents, the Fe_2O_3T content of other samples increases with increasing MgO content (Figure 6(b)). Most of the Hulu mineralized mafic–ultramafic samples have large losses on ignition (LOI) values (from 2.7 wt.% to 6.85 wt.%) because of alteration and high sulphide contents.

All the samples have chondrite-normalized rare earth element (REE) patterns enriched in light rare earth elements (LREEs) and display slightly negative or no Eu anomalies (Figure 7(a)). In the primitive mantle-normalized alteration-resistant trace element patterns, the samples are highly depleted in high field strength elements (HFSEs), particularly Ta and Nb, and enriched in large ion lithophile elements (LILEs) (Figure 7(b)).

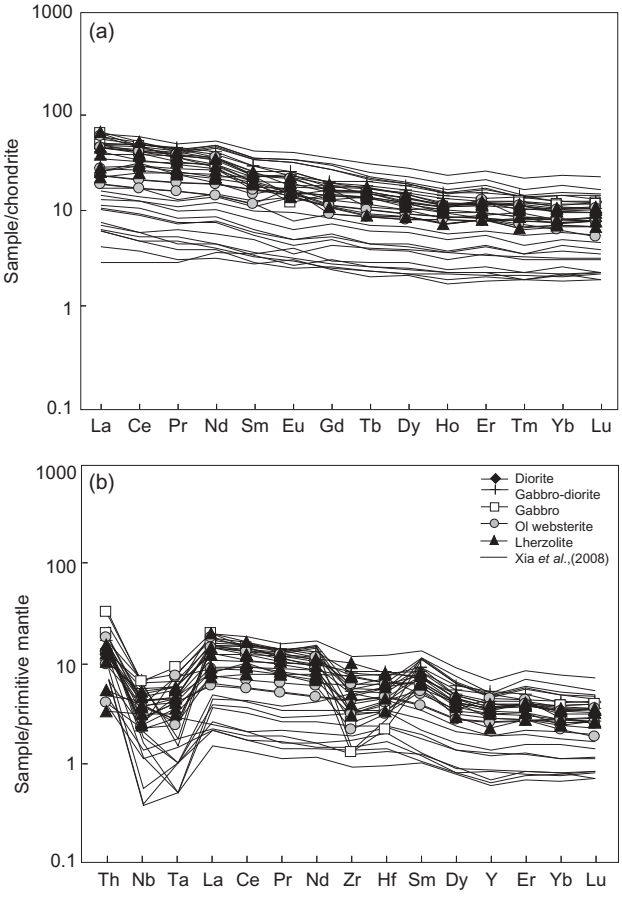

Figure 7. (a) Primitive mantle-normalized alteration-resistant trace element patterns and (b) chondrite-normalized REE patterns of the Hulu intrusive rocks. The chondrite values and primitive mantle values are from Taylor and McLennan (1985) and Sun and McDonough (1989), respectively.

Ni, Cu, and PGE abundances

The samples analysed in this study show low PGE contents (Table 2) relative to other magmatic Cu-Ni sulphide deposits worldwide. Os, Ir, Ru, Rh, Pt, and Pd contents are 0.03–0.77 ppb, 0.03–1.08 ppb, 0.04–0.67 ppb, 0.02–2.15 ppb, 0.05–34.5 ppb, and 0.18–344 ppb, respectively, and ΣPGE = 0.53–356.1 ppb. The sulphide-poor gabbro has the lowest Ni and Cu contents, whereas the sulphide-poor olivine websterite and lherzolite have higher Ni (0.07–0.09%) and Cu (0.01–0.03%) contents than the gabbro samples. The Cu and Ni abundances of the sulphide-bearing samples vary from 0.38% to 3.90% and 0.72% to 1.55%, respectively.

The massive sulphide samples contain higher contents of Pd, up to 344 ppb. Two Cu-rich massive sulphide samples have distinctly high Pd concentrations, whereas other samples show a positive relationship between Pt and Rh, and Pd and Ir (Figure 8(a) and (b)). The sulphide-rich rocks contain high S, ranging from 3.3 wt.% to 24.5 wt.%, whereas the S contents of the remaining sulphide-poor samples vary from 0.05 wt.% to 0.21 wt.%. Pd/Ir values vary from 4.75 to 27.7 in sulphide-poor samples and from 37.5 to 2436 in sulphide-rich samples. On the other hand, the Cu-rich massive ores have very high Pd/Ir values (1564–2436) because of their high Pd contents (Table 2). Pd/Pt values range from 0.28 to 1.08 in the sulphide-poor samples, and from 0.83 to 115.8 in the sulphide-rich samples. Apart from two massive sulphide samples, the data show a positive relationship of S with Pd, Ir, and Ni metals (Figure 8(d)–(f)). Cu/Pd values range from 60,000 to 480,000, with an average value of 180,000, which is significantly higher than the primitive mantle value of 7000 (Barnes and Maier 1999).

The primitive mantle-normalized chalcophile element patterns display a steep positive slope from Pd to Os (Figure 9). The sulphide-rich samples are notably depleted in Os, Ir, Ru, and Rh relative to Pt and Pd, but the depletion is not present in the sulphide-poor samples (Figure 9). Also, the disseminated and massive sulphide samples have slightly positive Rh anomalies and have relatively constant Ni but variable Cu tenors.

Sr-Nd isotope

The calculated initial $^{87}Sr/^{86}Sr$ values (t = 274 Ma, Sun *et al.* 2010) of the mafic–ultramafic rocks range from 0.7034 to 0.7048. $\varepsilon Nd(t)$ values of the Hulu intrusion are restricted within the range +5.7 to +8.8, with an average value of 7.3 (Table 3). The previously published Sr-Nd isotopes of Xia *et al.* (2008) (Figure 10) also show depleted mantle characteristics with higher $\varepsilon Nd(t)$ and lower initial $^{87}Sr/^{86}Sr$ values.

Table 2. Concentrations of Ni, Cu, S, and PGE in sulphide mineralized mafic–ultramafic rocks of the Hulu intrusion.

Sample No.		1090-5	1090-8	1005-12	1005-10	1005-20	965-1	1005-32	1005-31	1005-30	965-10	1005-11
Rocks		Gabbro	Gabbro	Pl-bearing Ol websterite	Lherzolite	Ol websterite	Lherzolite	Ol websterite	Ol websterite	Lherzolite	Ol websterite	Lherzolite
Mineralization		Sulphide-poor	Sparsely disseminated sulphide	Sulphide-poor	Sulphide-poor	Sulphide-poor	Net-textured sulphide	Disseminated sulphide	Disseminated sulphide	Disseminated sulphide	Massive sulphide	Massive sulphide
Cu	%	0.01	0.01	0.01	0.03	0.02	0.45	0.62	0.38	0.40	3.90	3.03
Ni	%	0.01	0.01	0.08	0.09	0.07	1.09	1.32	0.72	0.78	1.24	1.55
S	%	0.08	0.21	0.19	0.09	0.05	3.30	7.77	3.92	5.23	24.5	21.1
Pd	ppb	0.21	1.65	0.38	0.97	0.83	43.50	50.50	25.30	40.45	341.0	344.0
Pt	ppb	0.20	5.82	0.57	0.90	0.79	16.30	19.50	12.50	48.71	12.0	2.97
Rh	ppb	0.02	0.14	0.03	0.03	0.11	1.87	1.37	0.76	2.15	1.24	0.39
Ru	ppb	0.04	0.06	0.14	0.06	0.13	0.69	0.66	0.52	0.67	0.15	0.26
Ir	ppb	0.03	0.09	0.08	0.05	0.03	1.01	0.91	0.41	1.08	0.14	0.22
Os	ppb	0.03	0.18	–	0.09	0.03	0.41	0.77	0.27	–	0.35	0.22
∑PGE	ppb	0.53	7.94	1.00	2.10	1.92	63.8	73.7	39.8	93.1	355	348
Pd/Ir		7.0	18.3	4.8	19.4	27.7	43.1	55.5	61.7	37.5	2436	1564
Cu/Pd	$\times 10^7$	0.048	0.006	0.026	0.031	0.024	0.010	0.012	0.015	0.010	0.011	0.009
Pd/Pt		1.05	0.28	0.67	1.08	1.05	2.67	2.59	2.02	0.83	28.4	116
Ni/Cu		1.00	1.00	8.00	3.00	3.50	2.42	2.13	1.89	1.95	0.32	0.51
PPGE/IPGE		4.2	23.1	3.6	9.5	9.1	29.2	30.5	32.1	52.1	553.5	496.2
Elements in 100% sulphide												
100% Cu		4.7	1.8	1.9	12.7	15.2	5.0	3.0	3.6	2.9	6.0	5.4
100% Ni		4.7	1.8	15.2	38.0	53.2	12.0	6.4	6.9	5.6	1.9	2.8
100% S		37.6	38.5	36.2	32.3	30.3	36.4	37.6	37.4	37.7	37.9	37.9
100% Pd		98.8	302.3	72.4	409.6	630.8	479.5	244.1	241.4	291.6	528.2	617.5
100% Pt		94.1	1066.2	108.6	380.0	600.4	179.7	94.3	119.3	351.2	18.6	5.33
100% Rh		9.41	25.6	5.72	12.7	83.6	20.6	6.6	7.25	15.5	1.92	0.70
100% Ru		18.8	11.0	26.7	25.3	98.8	7.61	3.2	4.96	4.84	0.23	0.47
100% Ir		14.1	16.5	15.2	21.1	22.8	11.1	4.4	3.91	7.79	0.22	0.39
100% Os		14.1	33.0	–	38	22.8	4.5	3.7	2.58	–	0.54	0.39

Note: – below the detection limit.

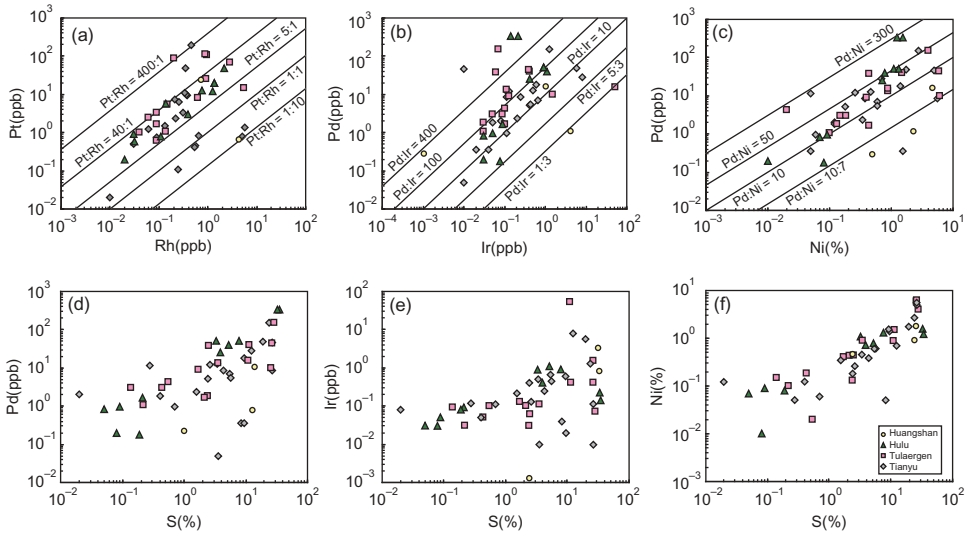

Figure 8. Plots of Pd *versus* Ir, Pt *versus* Rh, and S *versus* Pd and Ir for the Hulu mafic–ultramafic intrusion and the Permian magmatic sulphide deposits in the Eastern Tianshan. Data for the Tianyu deposit are from Tang *et al.* (2011); data for the Tulaergen and Huangshan are from unpublished data from Tang DM.

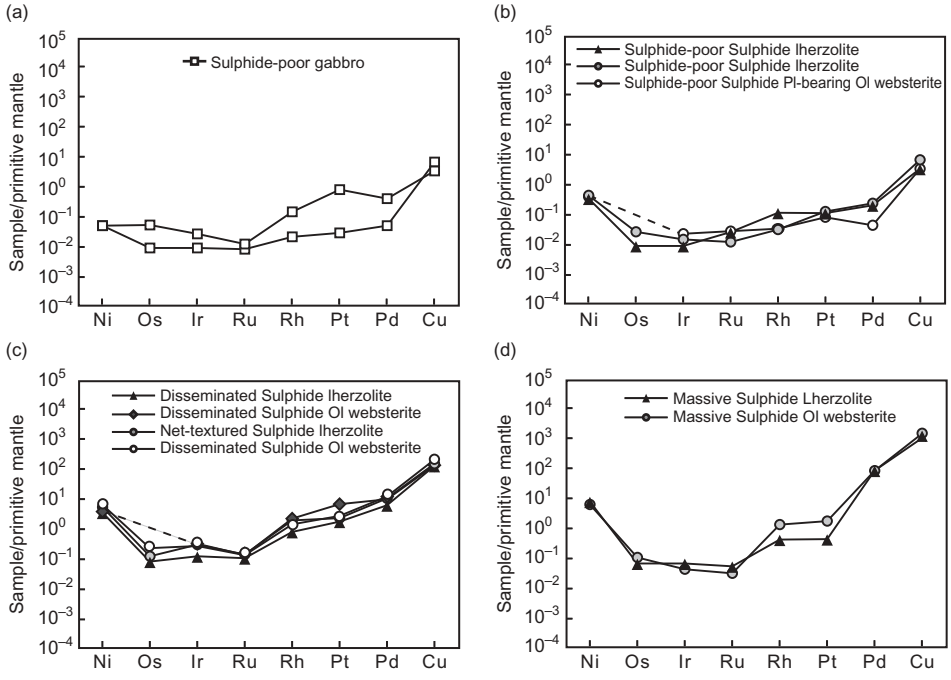

Figure 9. Primitive mantle-normalized chalcophile element patterns of the mafic–ultramafic rocks and sulphide ores. The primitive mantle values are from McDonough and Sun (1995).

S isotope

The $\delta^{34}S$ values of sulphides in the mafic–ultramafic rocks with different types of ores range from +1.5‰ to +4.9‰, whereas the values of the whole rocks vary from +3.7‰ to +5.1‰. The selected pyrite minerals and whole-rock powder of Carboniferous volcanic tuff have a relatively wide range of $\delta^{34}S$ values, from +1.8‰ to +6.7‰ (Table 4). The $\delta^{34}S$ values of sulphide and whole-rock are heavier than mantle sources (0 ± 2‰, Ohmoto and Rye 1979).

Discussion

Source characteristics and crustal contamination

The higher $\varepsilon Nd(t)$ values and lower initial $^{87}Sr/^{86}Sr$ values of the Hulu mafic–ultramafic rocks suggest that the

Table 3. Sr-Nd isotopic compositions of the Hulu mafic–ultramafic intrusion.

Sample No.	Rock	Rb (ppm)	Sr (ppm)	$^{87}Rb/^{86}Sr$	$^{87}Sr/^{86}Sr$	$\pm2\sigma$	$(^{87}Sr/^{86}Sr)_i$	Sm (ppm)	Nd (ppm)	$^{147}Sm/^{144}Nd$	$^{143}Nd/^{144}Nd$	$\pm2\sigma$	$\varepsilon Nd(t)$
1090-3	Gabbro-diorite	1.35	140	0.0490	0.705012	0.000008	0.704809	2.98	12.59	0.1475	0.512950	0.000012	7.81
1090-6	Gabbro-diorite	2.67	166	0.0645	0.704020	0.000009	0.703749	3.16	12.90	0.1638	0.512952	0.000013	7.28
1090-5	Gabbro	5.88	59.8	0.0285	0.703846	0.000018	0.703735	2.54	9.41	0.1634	0.512910	0.000009	6.48
1090-8	Gabbro	3.51	40.5	0.2505	0.704960	0.000010	0.703983	0.41	1.52	0.1611	0.513024	0.000015	8.78
1005-20	Ol websterite	1.91	21.7	0.0784	0.704086	0.000013	0.703780	0.67	2.43	0.1669	0.512876	0.000011	5.69
1005-31	Ol websterite	6.24	77.7	0.2325	0.704273	0.000012	0.703367	1.22	4.72	0.1565	0.512939	0.000008	7.28
1005-32	Ol websterite	4.88	56.0	0.2519	0.705032	0.000008	0.704050	0.48	1.80	0.1605	0.512949	0.000012	7.34
1005-12	Pl-bearing lherzolite	8.96	63.3	0.4097	0.704985	0.000013	0.703388	1.56	6.06	0.1555	0.512945	0.000019	7.44
1005-10	Lherzolite	3.23	30.2	0.3091	0.704723	0.000013	0.703518	0.46	1.76	0.1573	0.512923	0.000009	6.94
965-15	Lherzolite	2.91	80.3	0.0995	0.705005	0.000007	0.704612	0.93	3.31	0.1693	0.513001	0.000013	8.05

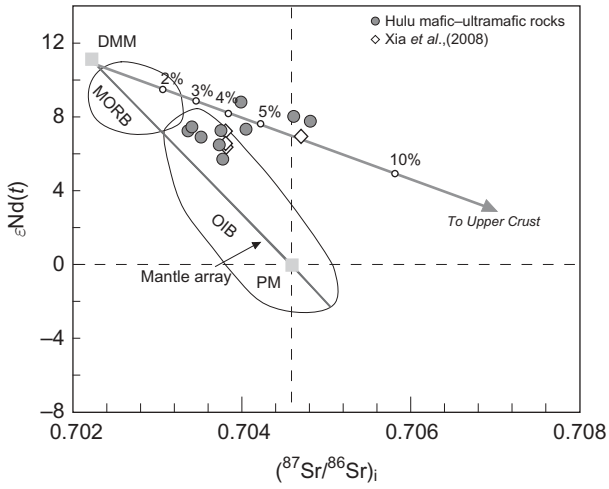

Figure 10. Plot of $\varepsilon Nd(t)$ *versus* $(^{87}Sr/^{86}Sr)_i$ for the Hulu mafic-ultramafic intrusion.

intrusion might have a depleted asthenospheric mantle source. The initial $^{87}Sr/^{86}Sr$ ranges (0.7033–0.7048) and high $\varepsilon Nd(t)$ values (+5.7 to +8.8) in the Hulu mafic–ultramafic rocks deviate from the mantle evolution trend (Figure 10), suggesting that the rocks might have experienced crustal contamination.

Assimilation of country rock is interpreted to have been a common phenomenon during the genesis of the Permian mafic–ultramafic related magmatic Ni-Cu sulphide deposits in the Jueluotage belt (Zhou *et al.* 2004; Chen *et al.* 2005; Chai *et al.* 2008; Tang *et al.* 2012). Crustal contamination can lead to the addition of external sulphur by means of devolatization, partial melting, or bulk assimilation of sulphide-bearing country rocks (Lesher and Campbell 1993; Ripley 1999), addition of external silica (Irvine 1975; Li and Naldrett 1993; Zhang *et al.* 2009a, 2009b), and an elevated oxygen fugacity (Haughton *et al.* 1974; Buchanan and Nolan 1979), all of which might have resulted in sulphur saturation of the magma.

The ratios of trace elements of similar partition coefficients (e.g. Ce/Pb, Th/Yb) can be accurately used to verify the role of assimilation (Jiang *et al.* 2006; Tang *et al.* 2012). The Ce/Pb values of the Hulu mafic–ultramafic rocks are 0.83–13.22, which are lower than the ratio of typical mantle (25 ± 5) but close to crustal values (<15, Hofmann 1997). Similarly, the Th/Yb values (+0.28 to +2.0) of the Hulu intrusion are also closer to average crustal values (3.7, Weaver and Tarney 1984) but significantly higher than that of the primitive mantle (0.17, Sun and McDonough 1989). The trends of mixing between the mantle and the upper and lower crusts are shown in Figure 11(a) and (b). Furthermore, the LILE/HFSE values higher than those of MORB, chondrite-normalized LREE enrichment, and flat HREE abundances indicate the addition of crustal material or subduction-related fluids (Figure 7). The $\varepsilon Nd(t)$ values and $(Th/Nb)_{PM}$ values of the Hulu mafic–ultramafic rocks are consistent with mixing between a depleted mantle-derived melt and the lower and upper crust, with mixing ratios of ~3% and 10%, respectively

Table 4. S isotopic characteristics in sulphide, whole rock, and country rocks of the Hulu Cu-Ni sulphide deposit.

Sample	Sample No.	Mineral/rock	$\delta^{34}S‰$
Sulphide in mafic–ultramafic rocks	965-3	Po	1.46
	965-3	Po	1.47
	965-3	Chp	1.83
	1005-3	Po	1.78
	1005-3	Chp	2.11
	965-4	Chp	4.87
	965-5	Chp	4.20
	1005-1	Chp	3.00
	965-3	Pen	4.30
Whole-rock	965-3	Disseminated sulphide lherzolite	3.73
	1005-17	Disseminated sulphide lherzolite	4.14
	1005-30	Disseminated sulphide lherzolite	3.69
	965-7	Sparsely disseminated sulphide ol websterite	5.13
	925-3	Diorite	3.58
Country rocks		Pyrite	1.94
		Pyrite	2.22
		Pyrite	2.92
		Pyrite	3.00
		Pyrite	3.44
		Pyrite	3.52
		Pyrite	1.80
		Tuff	6.70
		Tuff	5.60

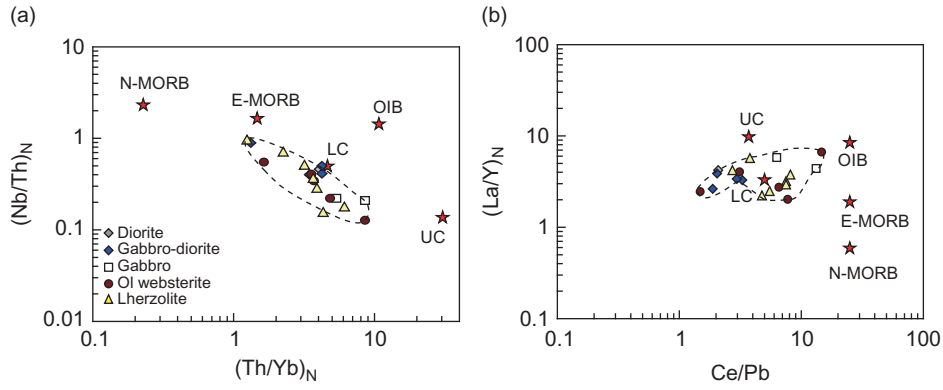

Figure 11. Plots of $(Th/Yb)_N$ *versus* $(Nb/Th)_N$ (a) and Ce/Pb *versus* $(La/Y)_N$ (b).

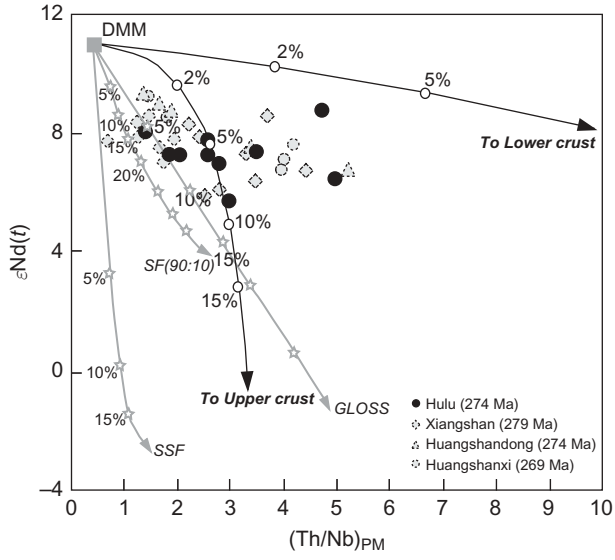

Figure 12. Plots of $\varepsilon Nd(t)$ *versus* $(Th/Nb)_{PM}$. The primitive mantle values are from McDonough and Sun (1995). The values for the depleted mantle-derived melt (DMM) represented by N-type MORB are from Sun and McDonough 1989, 2.33 ppm Nb, 0.12 ppm Th, $\varepsilon Nd(t)$ = 10.9; the values for the upper crust (UC) are from Rudnick and Gao (2003), 10.5 ppm Th, 12 ppm Nb, 27 ppm Nd, $\varepsilon Nd(t)$ = –10; the values for the coeval A-type granite in the region are from Wang *et al.* (2009). The values for the GLOSS are from Plank and Langmuir (1998), 6.91 ppm Th, 8.94 ppm Nb, 27 ppm Nd, $\varepsilon Nd(t)$ = –5.9, the values for SSF are from Johnson and Plank (1999), 3.69 ppm Nb, 1.233 ppm Th, 116.1 ppm Nd, $\varepsilon Nd(t)$ = –5.9, the values for SF are a mixture of 90% AOCF and 10% SSF, 2.51 ppm Nb, 0.98 ppm Th, 30.74 ppm Nd.

(Figure 12). However, the individual primitive mantle-normalized Th/Nb values are lower than the mixing model trend of both the upper and lower crust, but are identical to the Permian Xiangshan and Huangshan deposits in the Eastern Tianshan (Figure 12). Post-magmatic hydrothermal alteration had little effect on the Th contents of the samples, as indicated by a quantifiably positive correlation between the abundance of Th and the abundances of other immobile incompatible trace elements, such as REEs, in the samples. We thus propose that the low Th/Nb values may have resulted from subducted-zone fluids added to the magma source. We performed mixing calculations involving depleted mantle melt, global subducting sediments (GLOSS), slab fluid (SF), and subducted sediment fluid (SSF). The results suggest that the addition of ~5% melt from GLOSS and ~15% slab fluid to the initial magma could explain the $\varepsilon Nd(t)$ values and $(Th/Nb)_{PM}$ values of the Hulu intrusion (Figure 12). Such a regional characteristic of these Permian mafic–ultramafic intrusions in Eastern Tianshan may indicate the unusual composition of source mantle due to metasomatization by slab-derived fluids during subduction events (Zhou *et al.* 2004; Zhang *et al.* 2011; Tang *et al.* 2013). This may be the special feature of the magmatic deposits related to subduction and the later collision orogen structure setting in Eastern Tianshan. The addition of subducted-zone fluid in the magma source of the Eastern Tianshan area might decrease the melting point, and increase the partial melting degree of the mantle. The high partial melting primitive magma is favourable for magmatic sulphide deposit formation.

Early sulphide segregation and PGE-depleted parent magma

The palladium-group PGEs (PPGE)/iridium-group PGEs (IPGE) ratios of the Hulu mafic–ultramafic rocks vary from 3.6 to 23.1 in the sulphide-poor samples and from 29.2 to 553.5 in the sulphide-bearing samples, all of which are higher than the ratios of primitive mantle (~1, McDonough and Sun 1995) and of melt derived from 20% partial melting of primitive mantle (~18.6, Barnes and Lightfoot 2005).

Both Cu and Pd are siderophile elements, mainly controlled by the R-factor (mass ratio of silicate melt to sulphide melt; Campbell and Naldrett 1979) and the fractionation and segregation of residual sulphide liquid rather

than monosulphide solid solution (mss) or alloy (Crocket 1979; Fleet *et al.* 1996, 1999; Maier *et al.* 1996). Therefore, the whole-rock Cu/Pd value can be used as an indicator of the evolution of a single-pluse magma flow from the upper mantle (Brügmann *et al.* 1993). The higher Cu/Pd ratios of the sulphide-bearing samples, compared with the primitive mantle value of approximately 7000 (Barnes *et al.* 1988), could result in early sulphide segregation and PGE enrichment. Accordingly, the Cu/Pd values of 6×10^4 and 114×10^4 for the Hulu sulphide-poor and sulphide-bearing samples, respectively (Table 3), both of which are greater than 7000, suggest early sulphide segregation.

We estimate that the parent magma of the Hulu intrusion, composed of Pd (2.1 ppb), Os (0.03 ppb), Ir (0.05 ppb), and Cu (200 ppm), represents a MORB-like mantle (Crocket 2002). We therefore speculate that the PGE tenors in these samples represent an original sulphide liquid composition, and we subsequently used the mass balance equation of Campbell and Naldrett (1979) with these values and $D_{Pd}^{\text{sulphide/silicate melt}} = 30{,}000$, $D_{Os}^{\text{sulphide/silicate melt}} = 10{,}000$, $D_{Ir}^{\text{sulphide/silicate melt}} = 14{,}000$, and $D_{Cu}^{\text{sulphide/silicate melt}} = 1000$ (Francis 1990; Fleet *et al.* 1999) to model the generation of the melt. Our calculations indicate PGE contents after 0.01% sulphide segregation of Pd 0.4 ppb, Ir 0.01 ppb, and Os 0.01 ppb from MORB-like magma under an R-factor of 200–1600, or 0.005% sulphide segregation (Pd 0.5 ppb, Ir 0.02 ppb, Os 0.02 ppb) from that magma under an R-factor of 200–1600, can explain the Cu/Pd vs. Pd content in 100% sulphide of sulphide-poor and sparsely disseminated sulphide samples (Figure 13(a)). A variable R-factor of 200–1600, with residual magma that had experienced 0.01% early sulphide segregation, can explain the variations of Pd, Os, and Ir ratios in the sulphide-poor and disseminated sulphide samples (Figure 13(b) and (c)). In summary, the mineralized parental magma of the Hulu intrusion most likely experienced ~0.01% early sulphide segregation and became depleted in the PGE when it was emplaced into the shallow crust.

Formation of Hulu magmatic Ni-Cu sulphide deposit

There are various geodynamic models for the Permian mafic–ultramafic intrusions in Eastern Tianshan. These models include subduction-related processes (Xiao *et al.* 2004), post-collision extension (Mao *et al.* 2008; Yuan *et al.* 2010), or a mantle plume (Zhou *et al.* 2004; Wang

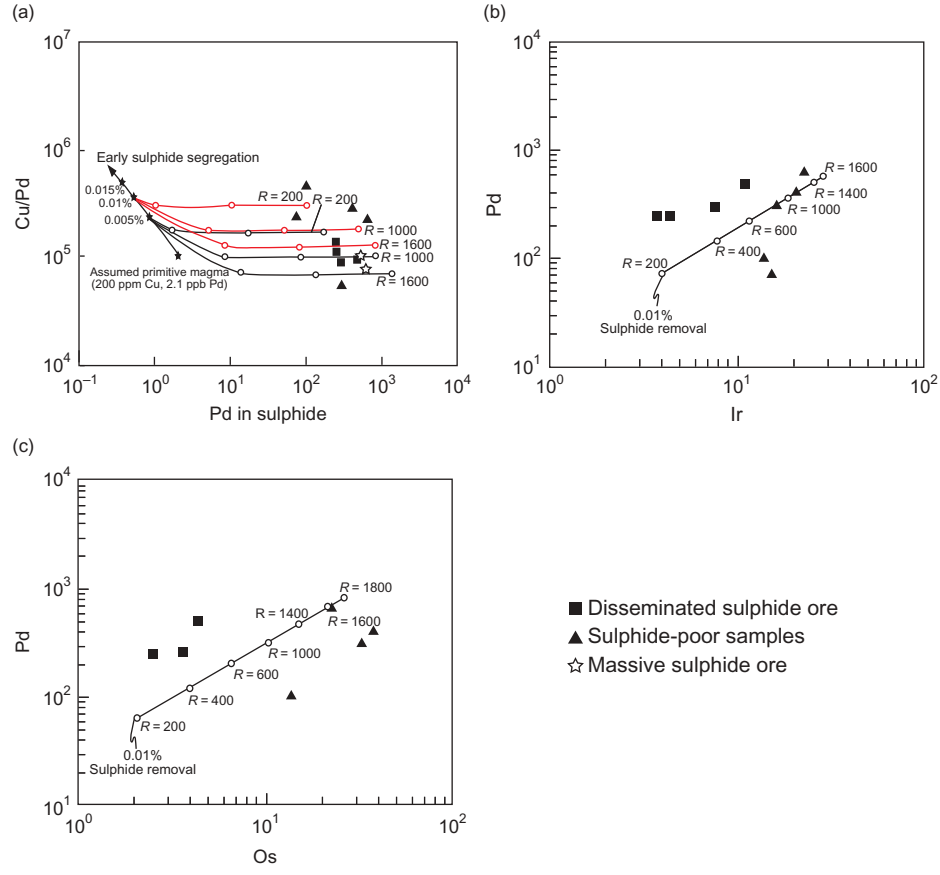

Figure 13. Model calculations of the Cu/Pd and Pd in 100% sulphide (a), Pd *versus* Ir (b), and Pd *versus* Os (c) of the recalculated 100% sulphide of the Hulu deposits. PGE variations in the sulphide ores of the Hulu intrusion can be reproduced using 0.02 ppb Ir, 0.02 ppb Os, and 0.5 ppb Pd (0.005% sulphide removal) and 0.01 ppb Ir, 0.02 ppb Os, and 0.4 ppb Pd (0.01% sulphide removal) in the parent magma.

et al. 2006; Pirajno *et al.* 2008; Zhang *et al.* 2010; Pirajno *et al.* 2011). However, recent studies proposed a mantle plume overlapping with subduction and/or orogen models (Qin *et al.* 2011; Su *et al.* 2011, 2012; Tang *et al.* 2013; Zhang and Zou 2013).

There are many studies on the Permian mafic–ultramafic intrusions in the Eastern Tianshan and the Tarim basalts, including spatial relationships, geophysics, geochronology, whole-rock major and trace element contents, Sr-Nd isotopic data, and parent magma compositions (Wang *et al.* 2006; Zhou *et al.* 2009; Tian *et al.* 2010; Zhang *et al.* 2010; Pirajno *et al.* 2011; Su *et al.* 2011; Xia *et al.* 2012; Zhang *et al.* 2013; Tang *et al.* 2013). Zhang and Zou (2013) further proposed that the Permian Tarim LIP has two different mantle domains for the coeval mafic–ultramafic rocks (the Tarim domain and the CAOB domain), according to the geochemistry of the mafic dikes. The Tarim domain is a long-term enriched continental lithospheric mantle, whereas the CAOB mantle is intensively depleted and variably enriched by Phanerozoic slab-derived fluids and/or subducted sediments.

Although the Hulu mafic–ultramafic intrusive rocks mainly experienced crustal contamination and the addition of subducted-zone fluids, the scenario that the PGE abundance in the crust and slab fluid and/or sediment is much lower than that of mantle plays little part in the PGE characteristics of the Eastern Tianshan mafic–ultramafic intrusive rocks. Thus, we used the PGE of the Hulu mafic rocks and Tarim basalts as an indicator of the original magma. Emeishan basalts and mafic–ultramafic intrusive rocks in Emeishan LIP are derived from the same mantle source. Furthermore, Emeishan mafic–ultramafic intrusions have magmatic Cu-Ni sulphide and independent magmatic PGE sulphide deposits (Xu *et al.* 2001, 2004; Song *et al.* 2003, 2006; Sun *et al.* 2008; Tao *et al.* 2008; Wang *et al.* 2010). Therefore, we compare the PGE, Cu, Ni, and ratio characteristics of Emeishan basalts, mafic–ultramafic related magmatic Cu-Ni-PGE deposits, Tarim basalts of Tarim LIP, and Hulu intrusive rocks of Eastern Tianshan.

Magmatic Ni-Cu sulphide deposits in the Emeishan LIP show higher Ni/Pd and Cu/Ir values than the Emeishan basalts and picrites, whereas the magmatic PGE-(Ni-Cu) sulphide deposits show apparently lower Cu/Ir and Ni/Pd values than the Emeishan basalt and picrites (Figure 14(a)). Cu/Ir and Ni/Pd values of these two types of deposits increase along the sulphide and PGM addition trend lines of the same basaltic magma from Barnes *et al.* (1993), respectively. The degree of Cu and Ni fractionation of magmatic Cu-Ni-PGE sulphide deposits is greater than that of the Emeishan basalts and picrites (Figure 14(b)). There is no Cu, Ni, and PGE evolution relationship between the Hulu mafic–ultramafic-related Cu-Ni sulphide deposits and the Tarim basalts. The Cu, Pd, and Ir contents of the Tarim basalts cannot be used as the mineralized magma to calculate the characteristic of Hulu deposits, under any R-factor or mass of sulphide segregation. However, Hulu deposit and Tarim basalts have similar Ni/Pd and Cu/Ir values (Figure 14(a)). Yuan *et al.* (2012) and Li *et al.* (2012a) showed that the Tarim basalts assimilated crustal material, became sulphur saturated and formed immiscible magmatic sulphides at depth. Therefore, we consider that both the Hulu deposit and Tarim basalts experienced early sulphide segregation and assimilation and/or contamination of crustal material, although the Hulu deposit did not fractionate and crystallize from the magma with Tarim basalt-like PGE characteristics directly.

The formation mechanism of the Hulu mafic–ultramafic intrusion was most likely partial melting of metasomatized depleted mantle by subducted slab-derived fluid or melt triggered by upwelling of the asthenosphere (Zhou *et al.* 2004; Gao *et al.* 2012; Tang *et al.* 2013). Both the fluids and upwelling led to an increased degree of partial melting, resulting in the generation of mafic magma, which is favourable for the formation of Cu-Ni sulphide deposits. A small degree of fractionation and 0.01% sulphide separation from the mineralized parental magma that settled to the bottom of the staging chamber or

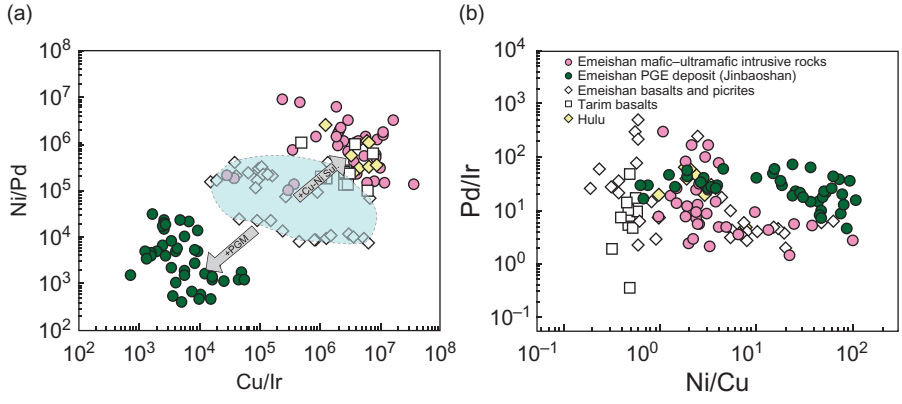

Figure 14. Plot of Cu/Ir *versus* Ni/Pd (a) and Ni/Cu *versus* Pd/Ir (b) in the Emeishan basalts/picrites, Ni-Cu-PGE sulphide deposits, Hulu deposits, and Tarim basalts. The data for the Emeishan intrusive rocks, basalts, and picrites are from Song *et al.* (2003, 2006), Tao *et al.* (2008), Sun *et al.* (2008), and Wang *et al.* (2010); data for Tarim basalts are from Li *et al.* (2012a, 2012b).

emplacement conduit can explain the depleted PGE content of the mineralized magma of the Hulu deposit. This early sulphide segregation event is very common in magmatic Ni-Cu sulphide deposits in northwest China and in the basalt and mafic–ultramafic intrusive rocks of the Emeishan area (Song *et al.* 2009; Wang *et al.* 2010; Song *et al.* 2011; Gao *et al.* 2012; Li *et al.* 2012a). The removal of sulphides resulted in the basaltic magma being depleted in the PGEs relative to Ni and Cu because of the high partition coefficient of the former. Thereafter, the evolved PGE-depleted magma ascended into the shallow magma chamber and intruded the sulphide-bearing tuff. Trace elements and Nd isotopic characteristics of the Hulu intrusion suggest that it had experienced both upper and lower crustal contaminations. Sulphide ores and whole rocks have higher $\delta^{34}S$ values than the mantle but similar to $\delta^{34}S$ values of country rocks, indicating the addition of higher $\delta^{34}S$ components. We propose that the basaltic magma underwent fractionation and assimilation of sulphur-bearing crustal materials, which triggered sulphur saturation and formed immiscible sulphide liquid. Finally, large amounts of sulphide melts were segregated to form the disseminated Cu-Ni sulphide ores.

Conclusions

The key findings of the present study are summarized as follows:

(1) The Hulu parental magma originated from depleted mantle, experienced ~5% subducting sediments and 15% slab fluid metasomatism, as well as approximately 3% lower crustal and 10% upper crustal contaminations. Addition of subducted zone fluids at source led to an increased degree of partial melting, which is favourable for the formation of Cu-Ni sulphide deposits.
(2) The Hulu mineralized magma experienced early 0.01–0.015% sulphide segregation and subsequently became depleted in PGEs to form the disseminated sulphide ores under R-factor values of 200–1600. Basaltic magma fractionation and assimilation of sulphur-bearing crustal materials might have triggered sulphur saturation and finally formed large amounts of Cu-Ni sulphide melts.
(3) Tarim basalt PGE concentrations cannot be used as the mineralized parent magma component of the Hulu deposit, but early sulphide segregation, assimilation and/or contamination of crustal material, and similar Cu/Ir, Ni/Pd, Cu/Ni, and Pd/Ir values imply that there is a certain relationship between them in magma source and composition.

Acknowledgements

We are grateful to Zhong-Li Tang, Zhuang-Zhi Qian, Chang-Yi Jiang, and Guang-Ming Li for providing information on the regional geology.

Funding

This study was financially supported by the Natural Science Foundation of China [Nos. 41002026 and 41030424] and China Postdoctoral Science Foundation-funded project to Dr Dong-Mei Tang.

References

Barnes, S.J., Boyd, R., Korneliusson, A., Nilsson, L.P., Often, M., Pedersen, B.B., and Robins, B., 1988, The use of mantle normalization and metal rations in discriminating between the effects of partial melting, crystal fractionation and sulphide segregation on platinum-group elements, gold, nickel and copper: Examples from Norway, *in* Prichard, H.M., Potts, P.J., Bowles, J.F.W., and Cribb, S.J., eds., Geo-Platinum: London, Elsevier, v. 87, p. 113–143.

Barnes, S.J., Couture, J.F., Sawyer, E.W., and Bouchaib, C., 1993, Nickel-copper occurrences in the Belleterre-Angliers Belt of the Pontiac subprovince and the use of Cu-Pd ratios in interpreting platinum-group element distributions: Economic Geology, v. 88, p. 1402–1418.

Barnes, S.J., and Lightfoot, P., 2005, The formation of magmatic nickel-copper-PGE sulphide deposits: Economic Geology, v. l90, p. 135–154.

Barnes, S.J., and Maier, W.D., 1999, The fractionation of Ni, Cu and the noble metals in silicate and sulphide liquids. *in* Keays, R.R., Lesher, C.M., Lightfoot, P.C., and Farrow, C.E.G., eds., Dynamic processes in magmatic ore deposits and their application to mineral exploration, short course notes: Geological Associate Canada v. 13, p. 69–106.

Brenan, J.M., and Li, C.S., 2000, Constraints on Oxygen fugacity during sulphide segregation in the Voisey's Bay intrusion, Labrador, Canada: Economic Geology, v. 95, p. 901–915.

Brügmann, G.E., Naldrett, A.J., Asif, M., Lightfoot, P.C., Gorbachev, N.S., and Fedorenko, V.A., 1993, Siderophile and chalcophile metals as tracers of the evolution of the Siberian Trap in the Noril'sk region, Russia: Geochimica et Cosmochimica Acta, v. 57, p. 2001–2018.

Buchanan, D.L., and Nolan, J., 1979, Solubility of sulphur and sulphide immiscibility in synthetic tholeiitic melts and their relevance to Bushveld Complex rocks: The Canadian Mineralogist, v. 17, p. 483–494.

Campbell, I.H., and Naldrett, A.J., 1979, The influence of silicate: Sulphide ratios on the geochemistry of magmatic sulphides: Economic Geology, v. 74, p. 1503–1505.

Chai, F.M., Zhang, Z.C., Mao, J.W., Dong, L.H., Zhang, Z.H., and Wu, H., 2008, Geology, petrology and geochemistry of the Baishiquan Ni-Cu-bearing mafic-ultramafic intrusions in Xinjiang, NW China: Implications for tectonics and genesis of ores: Journal of Asian Earth Sciences, v. 32, p. 218–235.

Chen, S.P., Wang, D.H., Qu, W.J., Chen, Z.H., and Gao, X.L., 2005, Geological features and ore formation of the Hulu Cu-Ni sulphide deposit, eastern Tianshan, Xinjiang: Xinjiang Geology, v. 23, p. 230–233. [In Chinese with English abstract.]

Chu, Z.Y., Chen, F.K., Yang, Y.H., and Guo, J.H., 2009, Precise determination of Sm, Nd concentrations and Nd isotopic

compositions at the nanogram level in geological samples by thermal ionization mass spectrometry: Journal of Analytical Atomic Spectrometry, v. 24, p. 1534–1544.
Coleman, R.G., 1989, Continental growth of Northwest China: Tectonics, v. 8, p. 621–635.
Crocket, J.H., 1979, Platinum-group elements in mafic and ultramafic rocks: Survey: Canadian Mineralogist, v. 17, p. 391–402.
Crocket, J.H., 2002, Platinum group element geochemistry of mafic and ultramafic rocks. In the Geology, Geochemistry, Mineralogy and Beneficiation of PGE, *in* Cabri, L.J., ed., CIM Spec: Montreal, QC, Canadian Institute of Mining, Metallurgy and Petroleum, v. 54, p. 177–210.
Fleet, M.E., Crocket, J.H., Liu, M.H., and Stone, W.E., 1999, Laboratory partitioning of platinum-group elements (PGE) and gold with application to magmatic sulphide-PGE deposits: Lithos, v. 47, p. 127–142.
Fleet, M.E., Crocket, J.H., and Stone, W.E., 1996, Partitioning of platinum-group elements (Os, Ir, Ru, Pt, Pd) and gold between sulphide liquid and basalt melt: Geochimica et Cosmochimica Acta, v. 60, p. 2397–2412.
Francis, R.D., 1990, Sulphide globules in mid-ocean ridge basalts (MORB) and the effect of oxygen abundance in Fe-S-O on the ability of those liquids to partition metals from MORB and komatiitic magmas: Chemical Geology, v. 85, p. 199–213.
Gao, J.F., Zhou, M.F., Lightfoot, P.C., Wang, C.Y., and Qi, L., 2012, Origin of PGE-poor and Cu-rich magmatic sulphide from the Kalatongke deposit, Xinjiang, Northwest China: Economic Geology, v. 107, p. 481–506.
Han, B.F., Ji, J.Q., Song, B., Chen, L.H., and Li, Z.H., 2004, SHRIMP zircon U-Pb ages of Kalatongke No. 1 and Huangshandong Cu-Ni-bearing mafic-ultramafic complexes, North Xinjiang and geological implications: Chinese Science Bulletin, v. 49, p. 2324–2328. [In Chinese.]
Haughton, D.R., Roeder, P.L., and Skinner, B.J., 1974, The solubility of sulphur in mafic magmas: Economic Geology, v. 69, p. 451–462.
Hofmann, A.W., 1997, Mantle geochemistry: The message from oceanic volcanism: Nature, v. 385, p. 219–229.
Irvine, T.N., 1975, Crystallization sequences in the Muskox intrusion and other layered intrusions-II. Origin of chromitite layers and similar deposits of other magmatic ores: Geochimica et Cosmochimica Acta, v. 39, p. 991–1020.
Jahn, B.M., Windley, B., Natal'in, B., and Dobretsov, N., 2004, Phanerozoic continental growth in Central Asia: Journal of Asian Earth Sciences, v.23, p. 599–603.
Jahn, B.M., Wu, F.Y., and Chen, B., 2000, Granitoids of the Central Asian Orogenic Belt and continental growth in the Phanerozoic. Transactions of the Royal Society of Edinburgh: Earth Sciences, v. 91, p. 181–193.
Jiang, C.Y., Cheng, S.L., Ye, S.F., Xia, M.Z., Jiang, H.B., and Dai, Y.C., 2006, Lithogeochemistry and petrogenesis of Zhongposhanbei mafic rock body at Beishan region, Xinjiang: Acta Petrologica Sinica, v. 22, p. 115–126. [In Chinese with English abstract.]
Johnson, M.C., and Plank, T., 1999, Dehydration and melting experiments constrain the fate of subducted sediments: Geochemistry, Geophysics, Geosystems, v. 1, p. 1–26.
Lesher, C.M., and Campbell, I.H., 1993, Geochemical and fluid-dynamic modeling of compositional variations in Archean komatiite-hosted nickel-sulphide ores in Western Australia: Economic Geology, v. 88, p. 804–816.
Li, Y.Q., Li, Z.L., Sun, Y.L., Santosh, M., Langmuir, C.H., Chen, H.L., Yang, S.F., Chen, Z.X., and Yu, X., 2012a, Platinum-group elements and geochemical characteristics of the Permian continental flood basalts in the Tarim Basin, northwest China: Implications for the evolution of the Tarim Large Igneous Province: Chemical Geology, v. 328, p. 278–289.
Li, C.S., and Naldrett, A.J., 1993, Sulphide capacity of magma: A quantitative model and its application to the formation of the sulphide ores at Sudbury: Economic Geology, v. 88, p. 1253–1260.
Li, C.S., Naldrett, A.J., and Ripley, E.M., 2001, Critical factor for the formation of a nickel-copper deposit in an evolved magma system: Lessons from a comparison of the Pants Lake and Voisey's Bay sulphide occurrences in Labrador, Canada: Mineralium Deposita, v.36, p. 85–92.
Li, C.S., Tao, Y., Qi, L., and Ripley, E.M., 2012b, Controls on PGE fractionation in the Emeishan picrites and basalts: Constraints from integrated lithophile-siderophile elements and Sr-Nd isotopes: Geochimica et Cosmochimica Acta, v. 90, p. 12–32.
Li, C.S., Zhang, M., Fu, P., Qian, Z., Hu, P., and Ripley, E.M., 2012c, The Kalatongke magmatic Ni-Cu deposits in the Central Asian Orogenic Belt, NW China: Product of slab window magmatism? Mineralium Deposita, v. 47, p. 51–67.
Lightfoot, P.C., and Keays, R.R., 2005, Siderophile and chalcophile metal variations in flood basalts from the Siberian Trap, Noril'sk Region: Implications for the origin of the Ni-Cu-PGE sulphide ores: Economic Geology, v. 100, p. 439–462.
Maier, W.D., 2005, Paltinum-group element (PGE) deposits and occurrences: Mineralization styles, genetic concepts, and exploration criteria: Journal of African Earth Sciences, v. 41, p. 165–191.
Maier, W.D., and Barnes, S.J., 1998, Concentrations of rare earth elements in silicate rocks of the Lower, Critical and Main Zones of the Bushveld Complex: Chemical Geology, v. 150, p. 85–103.
Maier, W.D., Barnes, S.J., De Klerk, W.J., Teigler, B., and Mitchell, A.A., 1996, Cu/Pd and Cu/Pt of silicate rocks in the Busheveld complex: Implications for platinum-group element exploration: Economic Geology, v. 91, p. 1151–1158.
Mao, J.W., Pirajno, F., Zhang, Z.H., Chai, F.M., Wu, H., Chen, S. P., Cheng, S.L., Yang, J.M., and Zhang, C.Q., 2008, A review of the Cu-Ni sulphide deposits in the Chinese Tianshan and Altay orogens (Xinjiang Autonomous Region, NW China): Principal characteristics and ore-forming processes: Journal of Asian Earth Science, v. 32, p. 184–203.
Mao, J.W., Yang, J.M., Qu, W.J., Wang, Z.L., and Han, C.M., 2002, Re-Os age of Cu-Ni ores from the Huangshandong Cu-Ni sulphide deposit in the East Tianshan Mountains and its implication for geodynamic processes: Mineral Deposits, v. 21, p. 323–330. [In Chinese with English abstract.]
McDonough, W.F., and Sun, S.S., 1995, The composition of the Earth: Chemical Geology, v. 120, p. 223–253.
Naldrett, A.J., 1989, Magmatic sulphide deposits: Oxford Monographs on Geology and Geophysics, v. 14, p. 186.
Naldrett, A.J., 2004, Magmatic sulphide deposits. Geology, geochemistry and exploration: Berlin, Springer, p. 1–727.
Ohmoto, H., and Rye, R.O., 1979, Isotopes of sulphur and carbon, *in* Barnes, H.L., ed., Geochemistry of hydrothermal ore deposits (second edition): New York, Wiley, p. 509–567.
Pirajno, F., Mao, J.W., Zhang, Z.C., Zhang, Z.H., and Chai, F.M., 2008, The association of mafic-ultramafic intrusions and A-type magmastism in the Tianshan and Altay orogens, NW China: Implications for geodynamic evolution and potential for the discovery of new ore deposits: Journal of Asian Earth Sciences, v. 32, p. 165–183.
Pirajno, F., Seltmann, R., and Yang, Y.Q., 2011, A review of mineral systems and associated tectonic settings of northern Xinjiang, NW China: Geoscience Frontiers, v. 2, p. 157–185.

Plank, T., and Langmuir, C.H., 1998, The chemical composition of subducting sediment and its consequences for the crust and mantle: Chemical Geology, v. 145, p. 325–394.

Qi, L., Zhou, M.F., Wang, C.Y., and Sun, M., 2007, An improved Carius tube technique for digesting geological samples in the determination of Re and PGEs: Geochemical Journal, v. 41, p. 407–414.

Qin, K.Z., Fang, T.H., and Wang, S.L., 2002, Plate tectonics division, evolution and metallogenic settings in eastern Tianshan mountains, NW China: Xinjiang Geology, v. 20, p. 302–308. [In Chinese with English abstract.]

Qin, K.Z., Su, B.X., Sakyi, P.A., Tang, D.M., Li, X.H., Sun, H., Xiao, Q.H., and Liu, P.P., 2011, SIMS zircon U-Pb geochronology and Sr-Nd isotopes of Ni-Cu-bearing mafic-ultramafic intrusions in eastern Tianshan and Beishan in correlation with flood basalts in Tarim Basin (NW China): Constraints on a ca. 280 Ma mantle plume: American Journal of Science, v. 311, p. 237–260.

Qin, K.Z., Zhang, L.C., and Xiao, W.J., 2003, Overview of major Au, Cu, Ni and Fe deposits and metallogenic evolution of the eastern Tianshan Mountains, Northwestern China, *in* Mao, J. W., and Goldfarb, S., eds., Tectonic evolution and metallogeny of the Chinese Altay and Tianshan: London, IA-GOD Guidebook Series 10:CERCAMS/NHM, p. 227–249.

Raczek, I., Stoll, B., Hofmann, A.W., and Jochum, K.P., 2001, High-precision trace element data for the USGS reference materials BCR-1, BCR-2, BHVO-1, BHVO-2, AGV-1, AGV-2, DTS-1, DTS-2, GSP-1 and GSP-2 by ID-TIMS and MIC- SSMS: Geostandards Newsletter, v. 25, p. 77–86.

Ripley, E.M., 1999, Systematics of sulphur and oxygen isotopes in mafic igneous rocks and related Cu-Ni-PGE mineralization, *in* Keays, R.R., Lesher, C.M., Lightfoot, P.C., and Farrow C.E.G., eds., Dynamic processes in magmatic ore deposits and their application to mineral exploration: Geological association of Canada: Short Course Notes v. 13 p. 133–158.

Ripley, E.M., Li, C.S., and Shin, D., 2002, Paragneiss assimilation in the genesis of magmatic Ni-Cu-Co sulphide mineralization at Voisey's Bay, Labrador: δ34S, δ13C and S/Se evidence: Economic Geology, v. 97, p. 1307–1318.

Ripley, E.M., Lightfoot, P.C., Li, C.S., and Elswick, E.R., 2003, Sulphur isotopic studies of continental flood basalts in the Noril'sk region: Implications for the association between lavas and ore-bearing intrusions: Geochimica et Cosmochimica Acta, v. 67, p. 2805–2817.

Rojas-Agramonte, Y., Kröner, A., Demoux, A., Xia, X., Wang, W., Donskaya, T., Liu, D., and Sun, M., 2011, Detrital and xenocrystic zircon ages from Neoproterozoic to Paleozoic arc terranes of Mongolia: Significance for the origin of crustal fragments in the Central Asian Orogenic Belt: Gondwana Research, v. 19, p. 751–763.

Rudnick, R.L., and Gao, S., 2003, Composition of the continental crust, *in* Rudnick, R.L., ed., Treatise on geochemistry: Oxford, Elsevier-Pergamon, p. 1–64.

Sengör, A.M.C., Natal'in, B.A., and Burtman, V.S., 1993, Evolution of the Altaid tectonic collage and Paleozoic crustal growth in Asia: Nature, v. 364, p. 299–307.

Song, X.Y., Keays, R.R., Zhou, M.F., Qi, L., Ihlenfeld, C., and Xiao, J.F., 2009, Siderophile and chalcophile elemental constraints on the origin of the Jinchuan Ni-Cu-(PGE) sulphide deposit, NW China: Geochimica et Cosmochimica Acta, v. 73, p. 404–424.

Song, X.Y., Xie, W., Deng, Y.F., Crawford, A.J., Zheng, W.Q., Zhou, G.F., Deng, G., Cheng, S.L., and Li, J., 2011, Slab break-off and the formation of Permian mafic-ultramafic intrusions in southern margin of Central Asian Orogenic Belt, Xinjiang, NW China: Lithos, v. 127, p. 128–143.

Song, X.Y., Zhou, M.F., Cao, Z.M., Sun, M., and Wang, Y.L., 2003, Ni-Cu-(PGE) magmatic sulphide deposits in the Yangliuping area, Permian Emeishan igneous province, SW China: Mineralium Deposita, v. 38, p. 831–843.

Song, X.Y., Zhou, M.F., Keays, R.R., Cao, Z.M., Sun, M., and Qi, L., 2006, Geochemistry of the Emeishan flood basalts at Yangliuping, Sichuan, SW China: Implications for sulphide segregation: Contribution to Mineralogy and Petrology, v. 152, p. 53–74.

Su, B.X., Qin, K.Z., Sakyi, P.A., Li, X.H., Yang, Y.H., Sun, H., Tang, D.M., Liu, P.P., Xiao, Q.H., and Malaviarachchi, S.P. K., 2011, U-Pb ages and Hf-O isotopes of zircons from Late Paleozoic mafic-ultramafic units in the southern Central Asian Orogenic Belt: Tectonic implications and evidence for an Early-Permian mantle plume: Gondwana Research, v. 20, p. 516–531.

Su, B.X., Qin, K.Z., Sun, H., Tang, D.M., Sakyi, P.A., Chu, Z.Y., Liu, P.P., and Xiao, Q.H., 2012, Subduction-induced mantle heterogeneity beneath Eastern Tianshan and Beishan: Insights from Nd-Sr-Hf-O isotopic mapping of Late Paleozoic mafic-ultramafic complexes: Lithos, v. 134–135, p. 41–51.

Su, B.X., Qin, K.Z., Tang, D.M., Sakyi, P.A., Liu, P.P., Sun, H., and Xiao, Q.H., 2013, Late Paleozoic mafic-ultramafic intrusions in southern Central Asian Orogenic Belt (NW China): Insight into magmatic Ni-Cu sulphide mineralization in orogenic setting: Ore Geology Reviews v, v. 51, p. 57–73.

Sun, S.S., and McDonough, W.F., 1989, Chemical and isotopic systematics in ocean basalt: Implication for mantle composition and processes, *in* Saunders, A.D., and Norry, M.J., eds., Magmatism in the Ocean Basins: Geological society of London: Special Publications, v. 42, p. 313–345.

Sun, T., Qian, Z.Z., Tang, Z.L., Jiang, C.Y., He, K., Sun, Y.L., Wang, J.Z., and Xia, M.Z., 2010, Zircon U-Pb chronology, platinum group element geochemistry characteristics of Hulu Cu-Ni deposit, East Xinjiang and its geological significance: Acta Petrologica Sinica, v. 26, p. 3339–3349. [In Chinese with English abstract.]

Sun, X.M., Wang, S.W., Sun, W.D., Shi, G.Y., Sun, Y.L., Xiong, D.X., Qu, W.J., and Du, A.D., 2008, PGE geochemistry and Re-Os dating of massive sulphide ores from the Baimazhai Cu-Ni deposit, Yunnan province, China: Lithos, v. 105, p. 12–24.

Sun, Y.L., Guan, X.Y., and Du, A.D., 1997, Preconcentration of precious metal elements by nickel sulphide fire assay□. Determination of platinum group elements in geological samples by ICP-MS: Rock and Mineral Analysis, v. 16, p. 21–26.

Tang, D.M., Qin, K.Z., Li, C.S., Qi, L., Su, B.X., and Qu, W.J., 2011, Zircon dating, Hf-Sr-Nd-Os isotopes and PGE geochemistry of the Tianyu sulphide-bearing mafic-ultramafic intrusion in the Central Asian Orogenic Belt, NW China: Lithos, v. 126, p. 84–98.

Tang, D.M., Qin, K.Z., Su, B.X., Sakyi, P.A., Liu, Y.S., Mao, Q., Santosh, M., and Ma, Y.G., 2013, Magma source and tectonics of the Xiangshanzhong mafic-ultramafic intrusion in the Central Asian Orogenic Belt, NW China, traced from geochemical and isotopic signatures: Lithos, v. 170, p. 144–163.

Tang, D.M., Qin, K.Z., Sun, H., Su, B.X., and Xiao, Q.H., 2012, The role of crustal contamination in the formation of Ni-Cu sulphide deposits in Eastern Tianshan, Xinjiang, Northwest China: Evidence from trace element geochemistry, Re-Os,

Sr-Nd, zircon Hf-O, and sulphur isotopes: Journal of Asian Earth Science, v. 49, p. 145–160.

Tao, Y., Li, C.S., Song, X.Y., and Ripley, E.W., 2008, Mineralogical, petrological, and geochemical studies of the Limahe mafic-ultramafic intrusion and associated Ni-Cu sulphide ores, SW China: Mineralium Deposita, v. 43, p. 849–872.

Taylor, S.R., and McLennan, S.M., 1985, The continental crust: Its composition and evolution: Oxford, Blackwell Publications, p. 312.

Tian, W., Campbell, I.H., Allen, C.M., Guan, P., Pan, W., Chen, M., Yu, H., and Zhu, W., 2010, The Tarim picrite-basalt-rhyolite suite, a Permian flood basalt from northwest China with contrasting rhyolites produced by fractional crystallization and anatexis: Contributions to Mineralogy and Petrology, v. 160, p. 407–425.

Wang, C.S., Gu, L.X., Zhang, Z.Z., Wu, C.Z., Tang, J.H., and Tang, X.Q., 2009, Petrogenesis and geological implications of the Permian high-K calc-alkaline granites in Harlik Mountains of eastern Tianshan, NW China: Acta Petrologica Sinica, v. 25, p. 1499–1511. [In Chinese with English abstract.]

Wang, C.Y., Zhou, M.F., and Qi, L., 2010, Origin of extremely PGE-rich mafic magma system: An example from the Jinbaoshan ultramafic sill, Emeishan large igneous province, SW China: Lithos, v. 119, p. 147–161.

Wang, J.B., Wang, Y.W., and He, Z.J., 2006, Ore deposits as a guide to the tectonic evolution in the East Tianshan mountains, NW China: Geology in China, v. 33, p. 461–469. [In Chinese with English abstract.]

Weaver, B.L., and Tarney, J., 1984, Empirical approach to estimation the composition of the continental crust: Nature, v. 310, p. 575.

Windley, B.F., Alexeiev, D., Xiao, W., Kroner, A., and Badarch, G., 2007, Tectonic models for accretion of the Central Asian Orogenic Belt: Journal of the Geological Society of London, v. 164, p. 31–47.

Windley, B.F., Kroner, A., Guo, J.H., Qu, G.S., Li, Y.Y., and Zhang, C., 2002, Neoproterozoic to Paleozoic geology of the Altai orogen, NW China: New zircon age data and tectonic evolution: Journal of Geology, v. 110, p. 719–737.

Wong, K., Sun, M., Zhao, G.C., Yuan, C., and Xiao, W.J., 2010, Geochemical and geochronological studies of the Alegedayi Ophiolitic Complex and its implication for the evolution of the Chinese Altai: Gondwana Research, v. 18, p. 438–454.

Wu, H., Li, H.Q., Mo, X.H., Chen, F.W., Lu, Y.F., Mei, Y.P., and Deng, G., 2005, Age of the Baishiquan mafic-ultramafic complex, Hami, Xinjiang and its geological significance: Acta Geologica Sinica, v. 79, p. 498–502. [In Chinese with English abstract.]

Xia, L.Q., Xu, X.Y., Li, X.M., Ma, Z.P., and Xia, Z.C., 2012, Reassessment of petrogenesis of Carboniferous-Early Permian rift-related volcanic rocks in the Chinese Tianshan and its neighboring areas: Geoscience Frontiers, v. 3, p. 445–471.

Xia, M.Z., Jiang, C.Y., Qian, Z.Z., Sun, T., Xia, Z.D., and Lu, R. H., 2008, Geochemistry and petrogenesis for Hulu intrusion in East Tianshan, Xinjiang: Acta Petrologica Sinica, v. 24, p. 2749–2760. [In Chinese with English abstract.]

Xiao, W.J., Windley, F., Huang, B.C., Han, C.M., Yuan, C., Chen, H.L., Sun, M., Sun, S., and Li, J.L., 2009, End-Permian to mid-Triassic termination of the accretionary processes of the southern Altaids: Implications for the geodynamic evolution, Phanerozoic continental growth, and metallogeny of Central Asia: International Journal of Earth Sciences, v. 98, p. 1189–1217.

Xiao, W.J., Zhang, L.C., Qin, K.Z., Sun, S., and Li, J.L., 2004, Paleozoic accretionary and collisional tectonics of the eastern Tianshan (China): Implications for the continental growth of central Asia: American Journal of Science, v. 304, p. 370–395.

Xu, X.W., Qin, K.Z., San, J.Z., Wang, Y., Hui, W.D., Kan, F., Mao, Q., Li, J.X., Sun, H., and Ma, Y.G., 2006, Discovery of layered mafic–ultramafic intrusive formed in 545 Ma in the Sidingheishan area, eastern Tianshan, China and its significances for tectonics and Cu-Ni mineralization: Acta Petrologica Sinica, v. 22, p. 2665–2676. [In Chinese with English abstract.]

Xu, Y.G., Chung, S.L., Jahn, B.M., and Wu, G.Y., 2001, Petrologic and geochemical constraintson the petrogenesis of Permian–Triassic Emeishan flood basalts in southwestern China: Lithos, v. 58(3–4), p. 145–168.

Xu, Y.G., He, B., Chung, S.L., Menzies, M.A., and Frey, F.A., 2004, Geologic, geochemical, and geophysical consequences of plume involvement in the Emeishan flood-basalt province: Geology, v. 32, p. 917–920.

Yuan, F., Zhou, T.F., Zhang, D.Y., Fan, Y., Liu, S., Peng, M.X., and Zhang, J.D., 2010, Source, evolution and tectonic setting of the basalts from the native copper mineralization area in the eastern Tianshan, Xinjiang: Acta Petrologica Sinica, v. 26, p. 533–546. [In Chinese with English abstract.]

Yuan, F., Zhou, T.F., Zhang, D.Y., Jowitt, S.M., Keays, R.R., Liu, S., and Fan, Y., 2012, Siderophile and chalcophile metal variations in basalts: Implications for the sulphide saturation history and Ni-Cu-PGE mineralization potential of the Tarim continental flood basalt province, Xinjiang Province, China: Ore Geology Reviews, v. 45, p. 5–15.

Zhang, C.L., and Zou, H.B., 2013, Comparison between the Permian mafic dykes in Tarim and the western part of Central Asian Orogenic Belt (CAOB), NW China: Implications for two mantle domains of the Permian Tarim Large Igneous Province: Lithos, v. 174, p. 15–27.

Zhang, C.L., Zou, H.B., Li, H.K., and Wang, H.Y., 2013, Tectonic framework and evolution of the Tarim block in NW China: Gondwana Research, v. 23, p. 1306–1315.

Zhang, M.J., Li, C.S., Fu, P., Hu, P.Q., and Ripley, E.M., 2011, The Permian Huangshanxi Cu-Ni deposit in western China: Intrusive-extrusive association, ore genesis and exploration implications: Mineralium Deposita, v. 46, p. 153–170.

Zhang, Y.T., Liu, J.Q., and Guo, Z.F., 2010, Permian basaltic rocks in the Tarim basin, NW China: Implications for plume-lithosphere interaction: Gondwana Research, v. 18, p. 596–610.

Zhang, Z.C., Mao, J.W., Chai, F.M., Yan, S.H., Chen, B.L., and Pirajno, F., 2009a, Geochemistry of the Permian Kalatongke mafic intrusions, Northern Xinjiang, NW China: Implications for the Genesis of the Magmatic Ni-Cu Sulphide Deposit: Economic Geology, v. 104(2), p. 185–203.

Zhang, Z.C., Mao, J.W., Saunders, A.D., Ai, Y., Li, Y., and Zhao, L., 2009b, Petrogenetic modeling of three mafic-ultramafic layered intrusions in the Emeishan large igneous province, SW China, based on isotopic and bulk chemical constraints: Lithos, v. 113, p. 369–392.

Zhang, Z.H., Mao, J.W., Du, A.D., Pirajno, F., Wang, Z.L., Chai, F.M., Zhang, Z.C., and Yang, J.M., 2008, Re-Os dating of two Cu-Ni sulphide deposits in northern Xinjiang, NW China and its geological significance: Journal of Asian Earth Sciences, v. 32, p. 204–217.

Zhou, M.F., Lesher, C.M., Yang, Z.X., Li, J.W., and Sun, M., 2004, Geochemistry and petrogenesis of 270 Ma Ni-

Cu-(PGE) sulphide-bearing mafic intrusions in the Huangshan district, Eastern Xinjiang, Northwest China: Implications for the tectonic evolution of the Central Asian orogenic belt: Chemical Geology, v. 209, p. 233–257.

Zhou, M.F., Zhao, J.H., Jiang, C.Y., Gao, J.F., Wang, W., and Yang, S.H., 2009, OIB-like, heterogeneous mantle sources of Permian basaltic magmatism in the western Tarim Basin, NW China: Implications for a possible Permian large igneous province: Lithos, v. 113, p. 583–594.